Managing the Interdisciplinary Requirements of 3D Geological Models

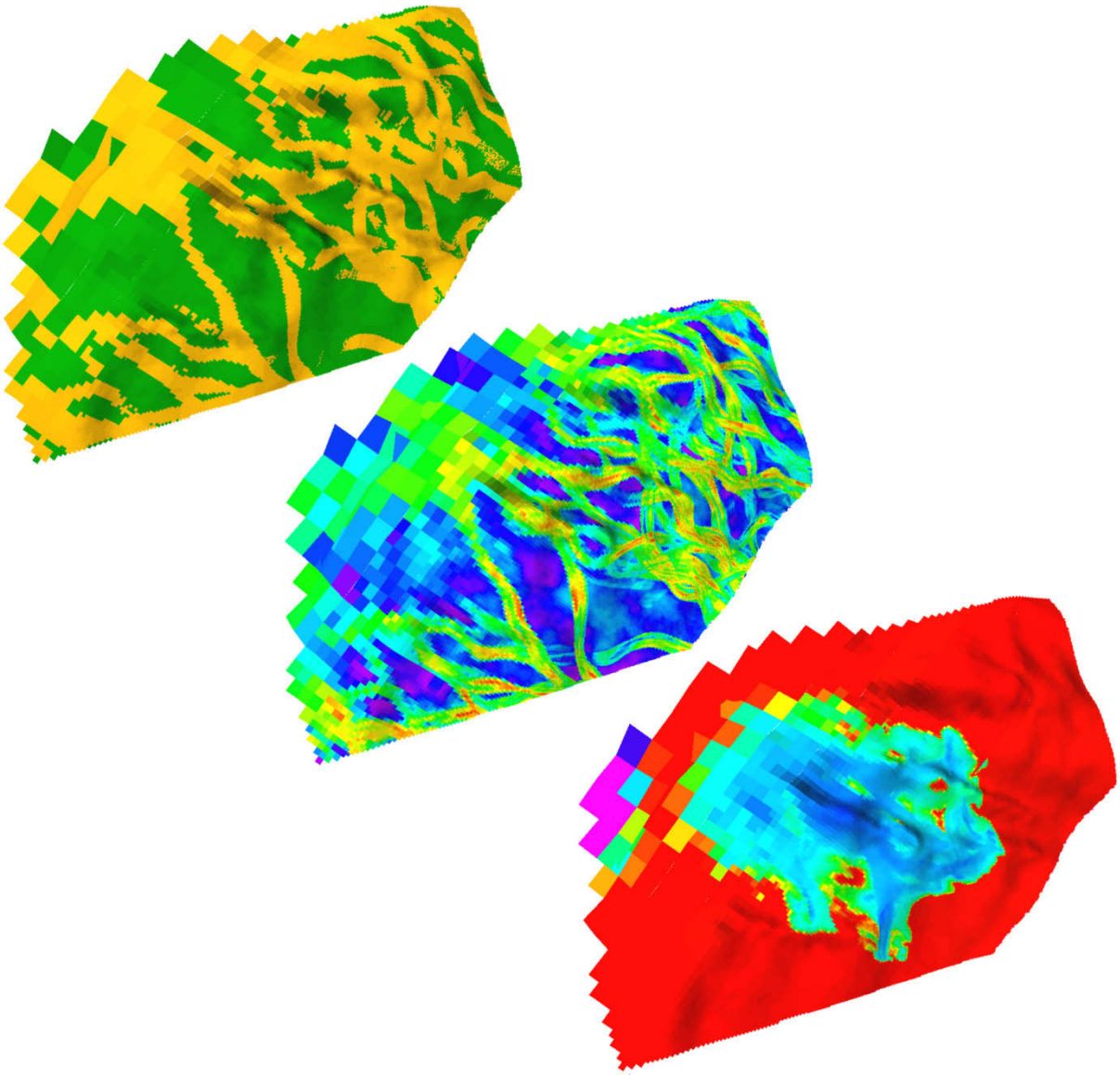

Sarah Jane Riordan
Australian School of Petroleum
University of Adelaide

March 2009

Thesis submitted in accordance with the requirements of the University of Adelaide

for the degree of Doctor in Philosophy

6 DYNAMIC MODELS

6.1 Introduction

Dynamic modelling was carried out in order to determine if the changes observed in static models (*Chapter 5*) as they are upscaled have a predictable influence on the behaviour of dynamic models. This chapter describes the dynamic models and examines the trends in production performance as grids are upscaled.

The dynamic modelling stage of this project was designed to study the influence of the geological model on the changes in reservoir simulation results as grids were upscaled. Weber and van Guens (1990) defined three types of reservoir: labyrinth, jigsaw and layer-cake. Labyrinth reservoirs have complex arrangements of sandbodies, often with poor connectivity (low net:gross) and fluid flow through these reservoirs will be dominated by sandbody connectivity. Jigsaw reservoirs have sand bodies that fit together without major gaps between them, but may have occasional low permeability zones that act as baffles to flow. Layer-cake type reservoirs have extensive, laterally continuous sandbodies that change gradually. Flow through layer-cake type reservoirs will be controlled by internal heterogeneities rather than sandbody connectivity (Peijs-van Hilten et al., 1998; Ringrose et al., 1999). Jian et al. (2002) studied the influence of permeability variogram length (an indicator of heterogeneity) on field production in a shoreface model. They found that variogram dimensions play a role in the timing of water breakthrough and consequently ultimate production. Models with large variograms had earlier water breakthrough compared to those with shorter variograms due to the lesser amount of heterogeneity in models with large variograms. However Kjønsvik et al. (1994) showed that parasequence offset and thickness are a primary control on waterflood performance, while Stephen et al. (2008) found that shoreface aggradation angle and curvature significantly influence simulation results. None of the aforementioned authors reported how changes to sandbody connectivity as a result of upscaling influenced the results of reservoir simulation studies. The models built for

this study fit into the category of labyrinth (channel scenarios) and layer-cake (coast scenarios).

As discussed in *Chapter 4*, a series of grids were built and populated with five geological scenarios (Figure 4.1). Once the base grids were upscaled, reservoir simulation was carried out. The same input parameters (rock properties, pressures, OWC) were used in all simulations, with only the grid design, porosity and permeability changing between grids. Rather than use the actual Flounder Field wells, many of which are deviated, five conceptual vertical wells were created for the reservoir simulation process. These were placed such that at the maximum level of upscaling they would still be within different grid blocks. The simulation pattern used is an inverted 5-spot pattern (a central injector, surrounded by four producers). This placement should ensure that the main controls on the results are either the grid design or the geology. As a control, to establish the influence of the underlying grid design, reservoir simulation was also carried out on a homogeneous model (all grid blocks have the same porosity and permeability values—15% and 1000 mD respectively), at all upscaling steps.

The final stage of the modelling process was to run reservoir simulation on the original, first generation model that honours the well data. This reservoir simulation was also carried out using the five conceptual vertical wells and the same input parameters (rock properties, OWC and production parameters) as the second generation theoretical models.

6.2 Methodology

Reservoir simulation was carried out using the 'Flowsim' module of RMS (Roxar, 2005). All scenarios used the five vertical wells that were created for the simulation process. The completion interval for the wells was the entire length of intersection with the grid. The distribution of the wells can be seen in (Figure 6.1). The well in the centre of the field (Well A) is the injector well, with the remaining wells (B, C, D & E) being the producers.

Reservoir simulation parameters were derived through experimentation on the homogeneous model. The aim was to have conditions that would produce water breakthrough in all wells in a time that would not take too long to simulate. A simulation period of 20 years was used. The reservoir pressure is slightly higher than that of the Flounder Field. The reservoir pressure has been increased as the interval modelled is lower than the main reservoir interval, and source of pressure data, in the field. The oil-water-contact has been lowered to minimize its impact on the results. The OWC was placed at the edge of the model, approximately 200 m deeper that the actual contact for the Flounder Field (Figure 6.1). Injection and production rates and wellbore pressures were all derived through trial and error without reference to field production data. Relative permeability curves, rock and fluid properties were left at RMS default values. These values resulted in the reservoir above the OWC having a uniform oil saturation of 80% at Time=0 for the reservoir simulation. The same conditions were applied to all grids and scenarios. It is assumed that by not changing production conditions, any changes in results will be attributable to changes in grid design and/or cell contents (geology).

The reservoir simulation process was carried out in three stages, as described below:

6.2.1 Stage 1

Reservoir simulation was run on a homogeneous model for each grid design, followed by three realizations of the geological models (Figure 4.1).

- All layer arrangements were modelled. Figure 6.2 shows which upscaled grid designs were simulated. Not all of the very fine grid designs were simulated due to time and computer memory constraints. Analysis of the results during this stage indicated that the detailed (small cell size) grids with 24 and 12 layers were likely to have very similar results to the 3 and 6-layer grids. The decision about which of the fine grids were simulated was based on the time taken to grid the next step up. For example, if the 120 x 160 x 24 grid took more than 72 hours to simulate, the 150 x 200 x 24 grid was not attempted. Grids that took more than 5 days to process were only simulated once.

- Plotted results, focusing on the changes in cumulative production between the grid sizes, and layers For a breakdown of the number of cells in grids, the cell dimensions and how that compared to channel widths see Table 6.1 and Table 6.2.

6.2.2 Stage 2

- Results from Stage 1 indicated that the 3-layer grid should provide representative results for the detailed (small cell size) grids. Seven more realizations were created for the channel and coast scenarios (total of 10 realizations) and upscaled to three layers.
- Reservoir simulations were run on realization 6–10 for 3-layer grids (Figure 6.2) in order to gain a better understanding of how upscaling influences production prediction.

6.2.3 Stage 3

- Reservoir simulations were run on 3 realizations of a model of the lower Roundhead Member that honoured the well data (1st generation model) in order to establish how well the conceptual models predicted the outcomes of real datasets.

6.2.4 Analysis

The following methods were used to analyze the results of the reservoir simulation:

1. comparison of ultimate field oil production
2. comparison of ultimate well production
3. comparison of cumulative oil and water recovery and water injection
4. connectivity of wells to channel facies
5. proximity of wells to porosity streaks
6. cell width to sandbody width ratio
7. % change between upscale grid production and base grid production
8. Sample correlation coefficient

1. *Ultimate Field Production*

The cumulative total field production at the end of 20 years was reported and analysed.

2. *Ultimate Well Production*

The total oil and water production (or water injection) for each well at the end of 20 years was reported and analysed.

3. *Cumulative Production and Injection*

The cumulative production (or injection) rates and recovery volumes were reported for each well for the 20 year production period.

4. *Channel Connectivity*

The volume of channel facies connected to each well was calculated inside RMS using the geometric connectivity function.

5. *Well Proximity to Porosity Streaks*

A method of assessing the proximity of the wells to the porosity streaks associated with channels was developed as a visual aid to understanding the interaction of channel size and location with well performance on a layer-by-layer basis. The facies model is a good indicator of channel proximity in the fine grids, but as the grids are upscaled (vertically or horizontally) this becomes less reliable as the porosity associated with the channels may persist in the grid after the channel facies has been lost as a result of the upscaling (Figure 6.3).

At each well location, the proximity of the blocked well to any channels was identified, and assigned a code (Figure 6.4). The categories are: channel centre, inside channel edge, outside channel edge, overbank, floodplain and bland. The last category (bland) caters for grids where the definition of the channel has been lost as a result of upscaling (this generally occurs once the grid cells exceed the width of the channels). A visual method, rather than a more precise numerical extraction of data from the grid is used as the definition of the channel edge becomes more difficult as the grids are upscaled. This method is highly interpretive, but does provide insight into the interactions between wells and the surrounding grid (Figure 6.4).

6. Cell to Sandbody Width Ratio

In order to compare results of dynamic models with different cell sizes the ratio of the cell width to sandbody width was calculated. This value, the *CSWR*, was used to enable statistical analysis of results from a wide variety of dynamic models.

- $CSWR = \frac{cell\ \ widt\ h}{sandbody\ \ \ widt\ h}$

7. %change

Another method for comparing results between models is the %change. This is the amount of production from an upscaled grid compared to the finest grid modelled.

- $\%change = \frac{upscaled\ \ \ grid\ \ production\ \ -base\ \ grid\ \ production}{base\ \ \ grid\ \ production}$

8. Sample correlation coefficient

The sample correlation coefficient (Devore, 1987) was calculated for each set of upscaled grids for each scenario and realization.

- $r = \frac{n\sum x_i y_i - (\sum x_i)\,(\sum y_i)}{\sqrt{n\sum x_i^2 - (\sum x_i)^2}\sqrt{n\sum y_i^2 - (\sum y_i)^2}}$

where n = *number of Realizations,*

x = *base model cumulative production, and*

y = *upscaled model cumulative production*

Realizations that have a large increase in production between grids are not excluded from the calculation of r even though some of them look like outliers and skew results. These sudden increases are a valid result, and occur at least once in most of the scenarios

6.3 Results

6.3.1 Homogeneous Model

The homogeneous model was included in the process to establish the underlying influence of grid design on simulation results. A trend was established in the results of the homogeneous

model as the grids were upscaled. It was anticipated that if the trends in results of the simulation of the geological models differ from this trend, the cause is most likely to be due to geological influences.

The simulation results for the homogeneous model indicated that the number of layers in the grid had little influence on the ultimate production from the grids (Figure 6.5). The similarity in results for the varying number of layers suggests that the x:z and y:z aspect ratio of the grids is not influencing the simulation outcomes for these grids (Figure 6.6).

The larger cell sizes (Figure 6.5,: blue-grey tint) show a decline in total oil production when the number of cells between the injecting well and at least one of the producing wells gets down to three cells or fewer (Figure 6.7, Figure 6.8 and Figure 6.9). In all grid designs this corresponds to the last three upscaling steps. This result would appear to conform to the 'rule of thumb' of Weber and van Guens (1990), which states that there should be at least three blocks between injection and producer pairs. There is approximately an 8% decrease in ultimate production between the finest grids simulated and the coarsest grids.

A closer look at the water influx behaviour in the square grid design indicates that in the early stages of the simulation (years 1 to 15) the water influx is radial which suggests that the structure of the grid is not influencing water flow behaviour at this time (Figure 6.10). Some distortion of the water front can be seen between years 15 and 20. The water front reaches Well E in the first year, followed by Well D, then Well B at around year 15 and finally Well C. Upscaling the grids horizontally has some impact on the water breakthrough time. The largest change (> 1 year difference) is seen between the 50 x 40 and the 25 x 20 grids. There is little difference in water breakthrough times as a result of vertical upscaling. The influence of the water breakthrough times can be clearly seen in the production profiles of the individual wells (Figure 6.11). Wells D and E produce significantly less oil than wells B and C, and their cumulative production curve flattens off as soon as the wells begin to produce water. As wells B and C have much later breakthrough, their recovery continues to climb throughout the production period.

The three grid designs (square, shoreface dip aligned (SDA) and shoreface strike aligned (SSA) have similar production for the grids with many cells, but the results diverge as the grids are upscaled horizontally (Figure 6.12). The differences in cell shape are apparent at the edge of the waterflood as the grids are upscaled (Figure 6.13, Figure 6.14 and Figure 6.15). The differences are also identifiable in the performance of individual wells. In the SDA grid the production profiles of Well E, the closest well to the producer, shows a clear change in ultimate oil recovery between the 60 x 20 grid and the 30 x 10 grid (Figure 6.16). In the 60 x 20 grid Well E is four cells away from the injector, and in the 30 x 10 grid it is 2 cells away. The clear difference in simulation results indicates that any simulation results for grids with 30 x 10 cells or fewer will be influenced by the interaction between grid design and well spacing. Similarly, the SSA grid results shows clear differences between the 30 x 40 grid and the 15 x 20 grid—the point at which there are three cells or fewer between the injector and producer (Figure 6.17).

6.3.2 Channel Scenarios

6.3.2.1 Vertical Upscaling

Analysis of the total field production for each of the channel scenarios indicates that, unlike the homogeneous models, there is deviation in simulation results as the grids are upscaled vertically as well as horizontally (Figure 6.18). In most cases the difference between the 24-layer grids and the 3-layer grids is less than 10% when there are more than three cells between the injector and producers. The difference increases significantly in the last three upscaling steps of all grids and scenarios. In all scenarios the channel thickness is between 2–8 m, with a mean of 5 m. As the average thickness of the cells is less than 5 m in all the grid designs, the average channel thickness should be greater than the average cell thickness. As noted in *section 5.2.2* there is some change to porosity distribution as a result of vertical upscaling.

6.3.2.2 Horizontal Upscaling

100 m channels, 25% gross sand (100-25)

In addition to realizations 1 to 3, realizations 4 to 10 were simulated for the 3-layer grid. The total field production for each realization of the 100 m scenarios is shown in Figure 6.19. The difference in field production between realizations is between $8x10^6$ m^3 and $12x10^6$ m^3 (lowest recovery is 15–25% of highest recovery) for the 25% gross sand scenario. The difference in total field production between realizations generally diminishes as the grids are upscaled.

A variety of trends are seen in the total field cumulative production as grid cell size changes. For the square grid design, the majority of realizations showed significant differences in the amount of oil produced between the finest grid and the coarsest grid (Figure 6.20). Four patterns of changes in ultimate production between upscaling steps are seen in the square grid design—which are considered representative of the behaviour for all the models:

1) Ultimate production changes with every upscaling step.
2) Ultimate production is relatively stable until the last three upscaling steps.
3) Ultimate production is stable only for the first 2–3 upscaling steps, and then changes significantly.
4) Ultimate production is stable for the first 4 upscaling grids, and then changes significantly.

1. Ultimate Production Changes With Every Upscaling Step

Realization 4 is representative of this pattern of upscaling results. The field cumulative production of Realization 4 changes with every upscaling step (Figure 6.21). A breakdown of production by well indicates that the majority of the production is coming from wells B and C (Figure 6.21). Wells D and E do not produce any oil until the grids are upscaled to 50 x 40 cells. In all wells there is a change in production trends between the 100 x 80 and the 50 x 50 grids (Figure 6.21). This realization has the following features:

- Channel connectivity: Well A (injector) is adjacent or penetrates a channel, and there are many channels in this part of the field (Figure 6.22 and Figure 6.5).
- Wells D and E do not penetrate any channels and are not close to any channels.

- Wells B and C are located adjacent to channels. As the grids are upscaled, the porosity at the wellbore changes from relatively poor (outside channel edge) to relatively good (inside channel edge) (Figure 6.23).
- The amount of water injected is relatively constant through all levels of upscaling (Figure 6.23 and Figure 6.24).
- Water influx occurs in an approximately radial pattern.

2. Ultimate Production is Relatively Stable Until The Last Three Grids

The field cumulative production for Realization 5 is representative of this pattern of results (Figure 6.25). This realization highlights the changes that occur to production when there are three cells or fewer between wells.

This realization has the following features:

- Wells A, B, E and D all penetrate channels in at least one layer (Figure 6.26).
- Well C does not penetrate any channels, and does not produce any oil until the 50 x 40 grid.
- Water influx follows a north-south trend (Figure 6.27).

3. Ultimate Production is Stable Only For The First 2–3 Upscaling Steps, And Then Changes

In Realization 9 the field cumulative production changes significantly after one upscaling step (Figure 6.28). This realization has the following features:

- Well A does not penetrate any channels in the base model (Figure 6.29).
- Wells C, D and E penetrate channels.
- As the grids are upscaled, the edge of a channel adjacent to Well A shifts, significantly changing the porosity at the Well A location (Figure 6.30).
- There is little water injection for first two upscaling steps, and water is not produced at the wells until the 200 x 100 grid (Figure 6.31).

4. Ultimate Production Is Stable For The First 4 Upscaling Grids, And Then Changes

Realizations 2 and 6 are representative of this pattern of results. Realization 2 has very poor production in the early upscaling steps, while Realization 6 has good production. (Figure 6.32). Realization 2 has the following features:

- This realization recovered the least oil of all the realizations.
- There are no channels near any of the wells (Figure 6.33 and Figure 6.34).
- Well A penetrates a low permeability area. There is minimal water influx until porosity becomes visually bland.
- The first four upscaling steps have very similar oil profiles and no water production.

In Realization 6 the total amount of oil produced is also stable for the first four upscaling grids and then increases in the 50 x 40 grid (Figure 6.35). This realization has the following features:

- It has one of the highest volumes of oil produced
- The injector and three of the producers penetrate the centre of a channel in at least one layer of the model (Figure 6.36)
- Water injection rates, which are relatively high, are similar for all grids except the 10 x 8 grid
- Water production begins early in Wells D and E

100 m channels, 50% gross sand (100-50): Realizations 1 to 10

The trends for total field production that are seen in the 100-25 models are also present when the amount of gross sand is increased (Figure 6.37). The difference in field production between realizations for the 100-50 models is $13x10^6$ to $20x10^6$ m^3 (lowest recovery is 10–30% of highest recovery), which is higher than the amount of variability seen in the 25% gross sand model. Overall the 50% gross sand models produce more oil than the 25% gross sand models—except when production is very low due to poor channel penetration. This results in a greater spread of potential field production values. The difference between

realizations once there are fewer than three cells between wells is less than is seen when there is only 25% gross sand.

In the square grid design, one realization stands out from the others with regards to the total field production. Realization 8 has very low production from the first two grids (500 x 400 and 250 x 200), after which production increases dramatically and stabilizes at a relatively high value (Figure 6.38). As was seen with the 100-25 models, the reason for the dramatic change in production is related to the position of the injector well relative to the channel sands (Figure 6.39). In this realization the injector is located away from the channel porosity, but as the grids are upscaled, the position of the channel edge shifts.

280 m channels (280-25 & 280-50): Realizations 1 to 10

The scenarios with wider channels allow the analysis of changes to simulation results as a result of upscaling while the cell size is less than the channel width. For square and SDA grids there are five grid sizes where the cell widths is less than or equal to the channel width (Table 6.2). In the square grid design the channel with equals the cell width in the 50 x 40 grid. The pattern of water flood for this scenario shows that in the 50 x 40 grid the channel boundaries are blurred and hard to identify (Figure 6.40). However there is not usually a significant shift in ultimate recovery between the 100 x 80 and the 50 x 40 grids (Figure 6.41).

As with the 100 m scenarios, variability in fine models—particularly large changes in production—are usually related to the position of the well(s) relative to channel margins. In the square grid design, 280-25 Realization 10 is highly variable (Figure 6.42). The spike in production in the 250 x 200 grid is the result of increased productivity in Well C. Well C is located in poor reservoir adjacent to a channel, and in the 250 x 200 grid, the upscaling is such that the cell containing the well shifts from the outside edge of the channel to the inside edge. This results in an increase in horizontal permeability (kh) at the well bore from 50 mD-m in the 500 x 400 grid to 1480 mD-m in the 250 x 200 grid, and back to 100 mD-m in the 200 x 160 grid.

The total field production from the SDA280-25 model stands out in that the majority of realizations have very stable production profiles (Figure 6.41). In this model, in most cases the injector is either located in an area of very poor porosity (low total production) or in the centre of a channel (high total production). There are few cases where the injector is located on the edge of a channel, and thus has significant changes in porosity and kh as the grids are upscaled.

6.3.3 Beach and Coast Scenario

6.3.3.1 Vertical Upscaling

As with the channel scenarios, the first step in the simulation process for the beach (shoreface only) and coast (shoreface and channels) scenarios was to compare the results of the 24-layer, 12-layer, 6-layer and 3-layer models from realizations 1 to 3 (Figure 6.43 and Figure 6.44). For both scenarios as grids are vertically upscaled there is some variation in total field production for grids with the same number of cells in the x and y direction. In all cases the difference between the 24-layer grids and the 3-layer grids is less than 10% when there are more than three cells between the injector and producers (Figure 6.45).

6.3.3.2 Horizontal Upscaling

The beach scenario has a variation in total field production of approximately $10x10^6$ m^3 (30%) between the realizations for both the square and SDA grids (this scenario was not run for the SSA grids) (Figure 6.44). As grids are upscaled horizontally there is usually little change in total field production between upscale steps (Figure 6.46). Where there is variation between grids, it is less than 10% of the value of the preceding grid (excluding the 25 x 20, 20 x 16 and 10 x 8 grids which are influenced by cell spacing). The pattern of water saturation due to the injection of water in Well A is consistent for all upscaling steps in this scenario (

Figure ***6.47***).

The coast scenario has approximately a $5x10^6$ m^3 variation in total field production between the three realizations for the square and SDA grid designs. There is very little variation

between realizations 1, 2 and 3 of the SSA grid (Figure 6.43). Ten realizations of the coast scenario for the 3-layer grid were run for all three grid designs (Figure 6.48). These show a variation in total field production of approximately 5–10x10^6 m^3 (14% variation for the SDA grid design and to 24% variation for the SSA and square grid designs). The total field production trends indicate that upscaling the grids has minor influence on the reservoir simulation performance for all grid designs. Variation between upscaling steps is usually less than 5% for the square and SSA grids and 10% for the SDA grids (Table 6.5).

A study of a the individual well production for the finest grids from each coast scenario 3–layer grid (SQ500 x 400, SSA300 x 400, SDA600 x 200 cells) shows that the majority of production is coming from Wells B and C—which are along strike from Well A, and penetrate mainly shoreface facies (Figure 6.49 and Figure 6.50). The relative contribution from Wells D and E varies between realizations, as the location of these wells is such that they do not always penetrate shoreface or channel facies (Figure 6.51 and Figure 6.52). In most cases the difference in contribution of wells to the total production varies less than 5% between grids in the same realization (excluding the 25 x 20, 20 x 16 and 10 x 8 grids which are influenced by cell spacing) (Table 6.4). This is in contrast to the 100 m channel scenario where there is up to 50% difference between grids (Table 6.3). There is less variability between grids for the production from wells B and C than for wells D and E (Figure 6.53). Injection volumes at well A are also fairly constant. The realizations that produce the greatest amount of oil from Well E (landward) usually penetrate a fluvial channel and/or the inside edge of the shoreface porosity in layer 3.

6.3.4 Lower Roundhead Scenario

Reservoir simulation was carried out on three realizations of the lower Roundhead Member model that honoured the actual Flounder field data (the reservoir simulation used the conceptual vertical wells that were created for simulating the conceptual models). Simulations were carried out on 24-layer, 12-layer, 6-layer and 3-layer grids (square design) (Figure 6.54). The variation in the ultimate production between the three realizations for the 3 layer 500 x 400 grid design is 1.9x10^6 m^3 (5% of maximum recovery—which is less than the

3.4 x10^6 m^3 (10%) variation seen in the equivalent conceptual coast scenario. There is also less variation between upscaled grids for the lower Roundhead scenario than for the square coastal scenario. The three realizations do not diverge significantly as the grids are upscaled.

When the field production is broken out into the individual wells, some variation between the upscaled grids is visible. The production patterns are the same as was seen in the conceptual wells. Wells D and E produce approximately 15% of the total field production, with the remaining production being split between wells B and C—Well B produces more than Well C (Figure 6.55). Well A, which has the same co-ordinates as Flounder A22 (Figure 6.56), shows very little variation between upscaled grids until the last three upscale stages. This well penetrates shoreface facies in all layers. The most variability between upscale steps is seen in Well B. This well penetrates channel facies in all layers (Figure 6.57). The width of the channel in this realization is approximately the same as the cell width in the 100 x 80 grid. The facies model shows that the cell at the wellbore changes from channel facies in the 100 x 80 grid to shoreface facies in the 50 x 40 grid. This is reflected in the porosity model with porosity increasing at the well bore between the two grids (Figure 6.58). The change in porosity of approximately 5% results in an increase in permeability at the wellbore in this layer from 274 mD-m to 1479 mD-m. Well B is located close to Flounder A20 which penetrates channel facies in all layers. This proximity has resulted in Well B also penetrating channel facies in all realizations. The ultimate production from Well B changes between the 100 x 80 and 50 x 40 grid in realizations 2 and 3 and between the 200 x 160 and 100 x 80 grid in realization 1. This suggests that the presence of the channel facies in this wellbore is influencing the performance of the well as the grids are upscaled.

6.3.5 Statistics

The changes in total field production as grids were upscaled were studied to find trends in behaviour. Refer to *section 6.2.4* for more detailed descriptions of terms.

6.3.5.1 Sample Correlation Coefficient vs. CSWR

The %change and the correlation coefficient were compared to the ratio of the cell width to the sandbody width (*CSWR*). By converting the relationship between cell width and sandbody width to a dimensionless number all grid designs and facies scenarios could be examined on one chart.

The sample correlation coefficient is a measure of the degree of linear relationship between two variables. When $r = 1$ all the variable pairs lie on a straight line with a positive slope. An r value between 1 and 0.8 indicates a strong correlation between the variables, while an r value less than or equal to 0.5 indicates a weak correlation (Devore, 1987). For the total field production there is a strong relationship between the base grid and upscaled grid when the *CSWR* is less than or equal to 0.4 (Figure 6.59). A moderate relationship (0.5 to 0.8) expected when the *CSWR* is between 0.4 and 0.75. This indicates that there is an increasing amount of uncertainty as the grids are upscaled to the width of the channel. Once the cell width is wider than the channel (*CSWR*>1) it is impossible to predict the potential relationship between the base grid production and the upscaled grid production as the results are extremely scattered.

For the coast scenario the calculation of *CSWR* was carried out using the width of the fluvial channels (280 m) and the width of the shoreface facies (2000 m). These data were compared with the *CSWR* of the beach scenario (shoreface only) and the channel scenario (Figure 6.60). This comparison indicates that the *CSWR* vs. r for the coast scenario is similar to that of the beach and channel scenarios when the width of the channels is used to calculate the *CSWR*. There is a strong relationship between the base grid and upscaled grid when the *CSWR* is less than or equal to 0.3. A moderate relationship between the base grid and the upscaled grid can be expected if the *CSWR* is between 0.4 and 0.75. If the *CSWR* is calculated using the shoreface facies width, the correlation coefficient of 0.5 is reached when the *CSWR* is 0.15—at which point the channel and beach scenarios have a correlation coefficient of more than 0.8.

Results from the lower Roundhead scenario were also included in this dataset (Figure 6.60). The lower Roundhead data falls on the same trend as the coast scenario data.

6.3.5.2 %Change vs. CSWR

The absolute change in ultimate recovery compared to the base model was also plotted against the *CSWR*. These data also showed that as the grids were upscaled, the variability in ultimate recovery increased. When the *CSWR* is less than 0.4 (the cut-off for $r \geq 0.8$) there is a less than 10% variation between the base grid and upscaled grid (Figure 6.61).

6.3.5.3 Base Grid Production vs. Upscaled Grid Production

The production from the upscaled grids was plotted against the production from the base grid. These plots indicate that as the grids are upscaled the gradient of the trend line through the data points shifts away from 1:1 (Figure 6.62). For realizations with relatively low production the ultimate field production is overestimated, while realizations with relatively high ultimate field production will be underestimated as the grids get bigger. These plots also highlight the increasing scatter of results once the *CSWR* exceeds 0.3.

6.4 Discussion – Dynamic Models

6.4.1 Discussion – Channel Scenarios

By breaking the total field production trends out into well production profiles it becomes apparent that the position of the wells relative to a channel is a critical control on the production profiles. Where there is good channel penetration of both the producers and the injector the results will be relatively insensitive to upscaling until the porosity grids change distribution. Similarly, where the wells do not penetrate close to channels, the results are most sensitive to gross changes in the porosity grid that results when the grids are upscaled beyond the width of the channels. Where wells penetrate the edge of channels, or adjacent to channels then significant changes in simulation results may occur when the cell size exceeds the channel width, and channel margins are altered by upscaling. Table 6.3 shows

that the relative contribution of each well to the total field production varies for each realization, and between grids of the same realization. There is no consistent point at which well contribution shifts significantly—cases of significant shifts in contribution can be found between all grid steps.

In this simulation design the injector has a significant influence on the field recovery. This is best illustrated in SQ100-25 Realization 9 where the injector does not penetrate a channel, and little water is injected until the porosity grids have been significantly altered by upscaling (Figure 6.29). Well C, which penetrates the centre of a channel, has a very different production profile in the non-injection case compared to the injection case (Figure 6.63 and Figure 6.64). Without injection the well looses production slightly as the grids are upscaled and porosity and permeability are decreased. With injection however, the well production increases significantly once the grids have been upscaled to the point that the porosity around the injector location is altered (Figure 6.30). In wells D and E the influence of injection is also seen in the water production profiles of the wells. In the no-injection case, they produce no water. Whereas in the injection case they produce water once the grids have been upscaled to the point at which Well A is capable of injecting significant volumes of water (Figure 6.29).

In some instances, one production property will be more obviously affected by upscaling than another. For example, in Realization 6, the cumulative oil production profiles show subtle changes between the 200 x 160 grid and the 100 x 80 grid. However, the water production profile for Well D shows a distinct change between these grids (Figure 6.35). The changes are also more obvious in the charts of oil rate than they are for cumulative production.

6.4.2 The influence of Channel Width and Cell Width on Production

In this study the reservoir properties of the wellbores are not fixed, but are extracted from the grids they penetrate—as would be this case when a simulation is used to predict the potential performance of planned wells. As a result, production is influenced by the changing of grid parameters as the grids are upscaled.

Changes in productivity between the grids where the *CSWR* is less than one are usually associated with the performance of one or more wells that are located close to the edge of a channel (Figure 6.23). As the grids are upscaled the edges of the channel related porosity shift slightly due to averaging effects. This has the potential to change the properties of any wells that are located near the margins of channels (shifting them either in or out of the channel porosity). Shifting channel margins is most likely to be an issue where cells are between half to one and a half times the channel width—as in these grids the channel porosity is still present and the overall porosity distribution is still fairly similar to that of the base grid.

Once the grids are upscaled to have greater width than approximately 1.5 times the channel width (SQ50 x 40, SDA60 x 20 and SSA60 x 80 grids) the porosity distribution shifts towards a normal distribution and becomes visually bland. The influence of this change in porosity distribution is easily recognized in realizations where few if any wells penetrate channel porosity—such as SQ100-25 Realization 2. SQ100-25 Realization 6, a good producer, also exhibits this behaviour in several wells (Figure 6.33 and Figure 6.36).

Realizations that show little change until the last three grids usually have the injector and at least one producer penetrating the centre of high quality channel porosity. The breakdown of performance by individual wells may show that all the situations described may be present, but high production from at least one well will dominate (Figure 6.25).

6.4.3 Discussion – Coast Scenario

The influence of channels within the shoreface facies is subtle, and difficult to quantify. In the square and SDA grid designs the width of the channels (280 m) is not exceeded until the last three grids—the results of which are unreliable. The plots of correlation coefficient vs. *CSWR* indicate that the grids with less than three cells between wells have a correlation coefficient of between 0 and 0.6—with most having a weak relationship ($r \leq 0.5$) (Figure 6.60 B). The *r* vs. *CSWR* plots suggest that channel width is likely to be influential on simulation results. The coast and lower Roundhead scenarios have a greater spread of *r* values than the beach

scenario (though this may be influenced by the small number of realizations of the beach scenario) (Figure 6.60 B).

The channels are identifiable within the shoreface facies by the change in direction of porosity trends (Figure 6.65). These trends diminish as the grids are upscaled and vanish once the *CSWR* exceeds 0.5 (Figure 6.65 part v). In the coast scenario channels have the same range of porosity as the shoreface facies, thus are not likely to act as either preferential conduits or baffles to flow. The subtle influence of channels within the shoreface can be seen in the water saturation model for the 500 x 400 x 3 grid (Figure 6.66). Changes in saturation that can be attributed to fluvial channels become more difficult to visually identify as the grids are upscaled (Figure 6.67 and Figure 6.68) and disappear before the cells reach the same width of the channels. The channels are usually only one layer thick in the 3-layer grid as their average thickness (2 m) is less than the average thickness of the cells (4 m).

There are changes in production performance between grids; however there is no consistent pattern to the variability between realizations or wells. As the influence of the position of wells relative to changes in porosity has been demonstrated in the channel models, the most likely explanation for the variability in the coast scenario is the position of wells relative to porosity sweet spots within the shoreface. The original Flounder porosity dataset has some very low porosity values (the result of carbonate cementation) that were not removed from the data set. As a result, the porosity models contain areas of very poor reservoir quality adjacent to areas of high reservoir quality.

6.4.4 Lower Roundhead Member simulation

The reservoir simulation carried out on the lower Roundhead Member model suggests that less variability between realizations can be expected when the grids honour well data. Although the conceptual wells (which do not have fixed reservoir properties) were used for the simulation, there is little variability at the well locations as they are located close to, or at, actual wellbores (Well D is an exception, but it penetrates offshore facies and has consistently poor reservoir quality). However, as was seen with the coast scenarios, three

realizations do not provide a good indication of the potential spread of production outcomes (Figure 6.43 and Figure 6.48) and these results should be treated with caution. The *CSWR* vs. *r* plots indicate that the lower Roundhead scenario results follow the same pattern as the coast scenario results. Thus, the channel widths appear to be influencing production. Analysis of the individual well performance suggests that the influence of channels can be identified in Well B. This well penetrates channels in all three realizations and shows a significant change in production when the cell width exceeds the channel width (Figure 6.55).

6.5 Conclusions – Dynamic Modelling

Any amount of upscaling has the potential to induce changes in field production compared to finer grids. Upscaling beyond the width of channels or significant flow path features is more likely to produce results that are different from those achieved with smaller cells. Within a series of realizations, where there is no control on well geology, a variety of behaviours can be expected:

- Wells that penetrate the centre of channels and are well connected to the injector may be relatively insensitive to upscaling (Figure 6.36).
- Wells that are located close to the edges of channels may have a significantly different response at every upscaling step (Figure 6.29).
- Wells that do not penetrate sand, or have poor sand content are likely to increase production when the porosity distribution becomes normal (bland) (Figure 6.33).
- If the cell width to channel width ratio (*CSRW*) is less than 0.3, then there is likely to be a strong correlation between the base grid and the upscaled grid, with less than 10% variation in ultimate recovery (Figure 6.61).
- If the cell width to channel width ratio (*CSRW*) is between 0.3 and 0.75, then there is a moderate to strong correlation between the base grid and the upscaled grid can be expected, with up to 20% variation in ultimate recovery (Figure 6.61).

- Once the cell width to channel width ratio (*CSRW*) exceeds 1.0 there is a high degree of variability between the base grid and the upscaled grid (Figure 6.61).

If the channel patterns cannot be seen clearly in the porosity model of a channel scenario, the ultimate production is likely to be different from what would be calculated for a smaller cell size.

The trends seen in the total field production are also seen in the performance of individual wells. At times, the sum of production from wells with varying upscaling patterns can produce an ultimate recovery pattern that is consistent at all levels of upscaling, yet individual wells may perform differently between upscaling steps. It is advisable to study the performance of individual wells as well as the total field performance.

6.6 Figures & Tables– Dynamic Modelling

SQUARE	№ CELLS	500 x 400	250 x 200	200 x 160	100 x 80	50 x 40	25 x 20	20 x 16	10 x 8
	x_M, y_M	28 x 24	56 x 48	70 x 60	140 x 120	280 x 240	560 x 480	700 x 600	1200 x 1400
SHOREFACE DIP ALIGNED	№ CELLS	600 x 200	300 x 100	240 x 80	120 x 40	60 x 20	30 x 10	24 x 80	12 x 4
	x_M, y_M	24 x 50	47 x 98	59 x 123	118 x 246	235 x 40	470 x 980	590 x 1230	1180 x 2460
SHOREFACE STRIKE ALIGNED	№ CELLS	300 x 400	150 x 200	120 x 160	60 x 80	30 x 40	15 x 20	12 x 16	6 x 8
	x_M,y_M	47 x 24	94 x 49	118 x 61	235 x 123	470 x 240	940 x 490	1180 x 610	2350 x 1230

Table 6.1. Grid design and cell dimensions and their relationship to channel widths. Orange shading indicates the grid designs that have cells that are less than 100 m wide in the x-direction. Channels are aligned to be approximately normal to the x-orientation of the cells. The blue-grey shading indicates where there are three cells or fewer between the injector and at least one producer. In these grids it is also likely that there will be less than three cells between wells and the edge of the grid.

SQUARE	№ CELLS	500 x 400	250 x 200	200 x 160	100 x 80	50 x 40	25 x 20	20 x 16	10 x 8
	x_M, y_M	28 x 24	56 x 48	70 x 60	140 x 120	280 x 240	560 x 480	700 x 600	1200 x 1400
SHOREFACE DIP ALIGNED	№ CELLS	600 x 200	300 x 100	240 x 80	120 x 40	60 x 20	30 x 10	24 x 80	2 x 4
	x_M, y_M	24 x 50	47 x 98	59 x 123	118 x 246	235 x 40	470 x 980	590 x 1230	1180 x 2460
SHOREFACE STRIKE ALIGNED	№ CELLS	300 x 400	150 x 200	120 x 160	60 x 80	30 x 40	15 x 20	12 x 16	6 x 8
	x_M,y_M	47 x 24	94 x 49	118 x 61	235 x 123	470 x 240	940 x 490	1180 x 610	2350 x 1230

Table 6.2. Grid design and cell dimensions and their relationship to channel widths. Purple shading indicates the grid designs that have cells that are equal to or less than 280 m wide in the x-direction. Channels are aligned to be approximately normal to the x-orientation of the cells. The blue-grey shading indicates where there are three cells or fewer between the injector and at least one producer. In these grids it is also likely that there will be less than three cells between wells and the edge of the grid.

Well Contribution to Total Production

.		500x400	250x200	200x160	100x80	50x40
Well B	R1	16%	28%	39%	26%	37%
	R2	31%	28%	29%	20%	6%
	R3	37%	40%	32%	22%	36%
	R4	34%	71%	80%	58%	33%
	R5	53%	40%	44%	44%	46%
	R6	9%	9%	8%	8%	9%
	R7	14%	13%	12%	14%	38%
	R8	51%	46%	45%	37%	35%
	R9	3%	4%	18%	32%	29%
	R10	18%	35%	21%	18%	26%

		500x400	250x200	200x160	100x80	50x40
Well C	R1	32%	23%	38%	25%	17%
	R2	12%	13%	12%	11%	26%
	R3	38%	36%	29%	23%	21%
	R4	56%	24%	15%	37%	43%
	R5	0%	0%	0%	0%	2%
	R6	43%	46%	45%	48%	49%
	R7	22%	23%	37%	35%	22%
	R8	42%	35%	32%	35%	33%
	R9	20%	22%	27%	38%	25%
	R10	39%	27%	36%	35%	28%

		500x400	250x200	200x160	100x80	50x40
Well D	R1	17%	14%	10%	26%	31%
	R2	27%	28%	31%	29%	17%
	R3	5%	7%	14%	32%	22%
	R4	5%	3%	3%	2%	8%
	R5	31%	35%	38%	41%	33%
	R6	26%	27%	26%	25%	27%
	R7	19%	18%	14%	16%	10%
	R8	4%	16%	22%	16%	21%
	R9	46%	43%	33%	20%	27%
	R10	36%	34%	40%	42%	38%

		500x400	250x200	200x160	100x80	50x40
Well E	R1	35%	35%	13%	23%	15%
	R2	30%	31%	27%	40%	51%
	R3	20%	18%	25%	23%	21%
	R4	4%	2%	2%	3%	16%
	R5	15%	25%	17%	15%	19%
	R6	22%	18%	21%	18%	15%
	R7	45%	47%	37%	35%	30%
	R8	4%	4%	2%	11%	10%
	R9	31%	31%	21%	9%	19%
	R10	7%	5%	3%	4%	8%

Table 6.3. Contribution of wells to total field production. Square grid, 100-25, 3 layers. The black line on the table highlights the point at which cell size exceeds channel width. While in some wells, such as R3 Wells D and B, there is a significant change in the wells contribution to the field production between the 200 x 160 and the 100 x 80 grids, it is not consistent and significant differences between other grids are also common.

The colours highlight the variability in production contribution and the colour scale (green high values, red low values) is applied to all the realizations in a well.

Well Contribution to Total Production

		500x400	250x200	200x160	100x80	50x40
Well B	R1	46%	48%	48%	46%	49%
	R2	47%	47%	47%	48%	45%
	R3	34%	35%	37%	35%	39%
	R4	45%	45%	44%	45%	43%
	R5	41%	41%	43%	43%	43%
	R6	43%	45%	46%	43%	51%
	R7	50%	50%	48%	48%	53%
	R8	51%	50%	51%	52%	53%
	R9	43%	43%	43%	44%	44%
	R10	51%	53%	52%	52%	51%

		500x400	250x200	200x160	100x80	50x40
Well C	R1	48%	46%	47%	47%	45%
	R2	48%	49%	49%	46%	51%
	R3	47%	48%	48%	45%	45%
	R4	41%	42%	41%	40%	45%
	R5	48%	48%	47%	49%	49%
	R6	48%	49%	48%	48%	41%
	R7	39%	39%	39%	40%	35%
	R8	44%	44%	44%	42%	42%
	R9	49%	49%	50%	49%	49%
	R10	30%	30%	31%	34%	35%

		500x400	250x200	200x160	100x80	50x40
Well D	R1	4%	4%	4%	3%	3%
	R2	2%	2%	2%	2%	2%
	R3	12%	10%	10%	13%	10%
	R4	10%	9%	10%	9%	7%
	R5	5%	5%	5%	4%	4%
	R6	4%	3%	3%	3%	2%
	R7	10%	9%	11%	9%	10%
	R8	4%	4%	4%	3%	3%
	R9	3%	3%	3%	3%	3%
	R10	5%	5%	6%	5%	5%

		500x400	250x200	200x160	100x80	50x40
Well E	R1	2%	2%	1%	3%	3%
	R2	2%	2%	2%	4%	2%
	R3	7%	7%	6%	7%	6%
	R4	4%	4%	6%	5%	6%
	R5	6%	6%	5%	4%	5%
	R6	5%	3%	3%	7%	6%
	R7	1%	1%	2%	3%	2%
	R8	1%	1%	1%	2%	2%
	R9	5%	5%	4%	5%	5%
	R10	14%	13%	12%	10%	9%

Table 6.4. Breakdown of individual well contribution to total field production—square grid, coast scenario, 3 layers. This shows that there is generally less than 5% variation in total production between the grids at different levels of upscaling. In this scenario the influence of the shoreface facies dominates production.

The colours highlight the variability in production contribution and the colour scale (green high values, red low values) is applied to all the realizations in a well.

		250x200	200x160	100x80	50x40	25x20	20x16
Square Model	R1	3%	2%	2%	3%	8%	1%
	R2	2%	0%	3%	6%	3%	4%
	R3	2%	2%	4%	4%	11%	4%
	R4	6%	2%	3%	2%	7%	1%
	R5	2%	2%	1%	1%	4%	0%
	R6	1%	3%	1%	9%	17%	6%
	R7	4%	4%	1%	0%	4%	4%
	R8	2%	1%	1%	3%	1%	2%
	R9	3%	1%	4%	2%	8%	11%
	R10	4%	3%	1%	4%	5%	2%

		300x100	240x80	120x40	60x20	60x20	24x8
Shoreface Dip Aligned	R1	8%	6%	7%	11%	11%	6%
	R2	0%	5%	8%	2%	2%	2%
	R3	5%	6%	4%	5%	5%	3%
	R4	4%	3%	6%	3%	3%	2%
	R5	5%	2%	6%	3%	3%	2%
	R6	5%	3%	4%	1%	1%	4%
	R7	5%	3%	0%	2%	2%	3%
	R8	1%	1%	1%	5%	5%	1%
	R9	1%	1%	3%	7%	7%	4%
	R10	2%	3%	1%	2%	2%	0%

		150x200	120x160	60x80	30x40	15x20	12x16
Shoreface Strike Aligned	R1	3%	3%	1%	7%	3%	3%
	R2	3%	3%	3%	4%	7%	7%
	R3	0%	4%	1%	3%	1%	11%
	R4	2%	3%	3%	2%	8%	11%
	R5	5%	3%	5%	16%	18%	12%
	R6	2%	1%	1%	5%	21%	22%
	R7	4%	0%	3%	1%	12%	8%
	R8	3%	1%	0%	4%	17%	9%
	R9	3%	9%	0%	2%	23%	36%
	R10	3%	2%	0%	4%	11%	13%

Table 6.5. Coast scenario—a comparison of the relative change in field production between a grid and its preceding one. For example there is a 2% change on field production between the 200 x 160 grid and the 250 x 200 grid in Realization 1 of the square grid. These tables show that where there are more than 3 cells between Well A and the other wells (cells to the left of the heavy black line) there is generally less than 5% difference between grids. There is slightly more variability in the SDA grid than in the square and SSA grids.

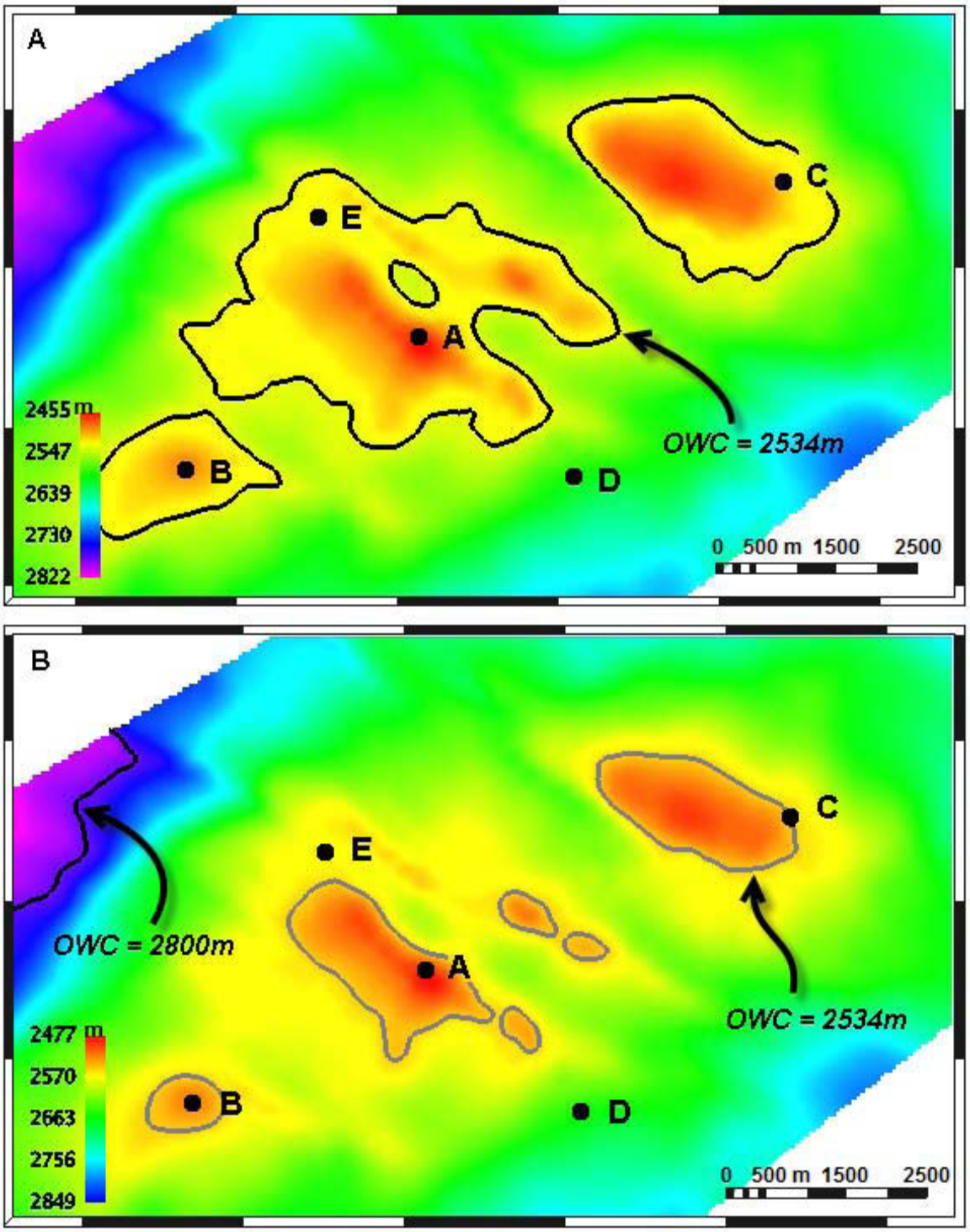

Figure 6.1. Depth structures and Oil Water Contacts. Figure A shows the depth at the top of the main reservoir interval—the RU.4 unit. Figure B shows the depth at the top of the interval modelled—the RL.6 unit. At this depth, there is little section above the OWC. In order to minimize the impact of the OWC on the results of the reservoir simulation, the OWC in the simulation setup has been lowered to 2800 m at the edge of the model.

Square Model

Grid Blocks / Layers	1000x800	500x400	250x200	200x160	100x80	50x40	25x20	20x16	10x8
24	Base		R1* R2* R3*	R1 R2 R3	R1 R2 R3	R1 R2 R3	R1 R2 R3	R1 R2 R3	R1 R2 R3
12			R1* R2* R3*	R1 R2 R3	R1 R2 R3	R1 R2 R3	R1 R2 R3	R1 R2 R3	R1 R2 R3
6			R1* R2* R3*	R1 R2 R3	R1 R2 R3	R1 R2 R3	R1 R2 R3	R1 R2 R3	R1 R2 R3
3		R1 R2 R3 R4 R5 R6 R7 R8 R9 R10	R1 R2 R3 R4 R5 R6 R7 R8 R9 R10	R1 R2 R3 R4 R5 R6 R7 R8 R9 R10	R1 R2 R3 R4 R5 R6 R7 R8 R9 R10	R1 R2 R3 R4 R5 R6 R7 R8 R9 R10	R1 R2 R3 R4 R5 R6 R7 R8 R9 R10	R1 R2 R3 R4 R5 R6 R7 R8 R9 R10	R1 R2 R3 R4 R5 R6 R7 R8 R9 R10

Shoreface Strike Aligned Model

Grid Blocks / Layers	600x800	300x400	150x200	120x160	60x80	30x40	15x20	12x16	6x8
24	Base		R1 R2 R3	R1 R2 R3	R1 R2 R3	R1 R2 R3	R1 R2 R3	R1 R2 R3	R1 R2 R3
12			R1 R2 R3	R1 R2 R3	R1 R2 R3	R1 R2 R3	R1 R2 R3	R1 R2 R3	R1 R2 R3
6			R1 R2 R3	R1 R2 R3	R1 R2 R3	R1 R2 R3	R1 R2 R3	R1 R2 R3	R1 R2 R3
3		R1 R2 R3 R4 R5 R6 R7 R8 R9 R10	R1 R2 R3 R4 R5 R6 R7 R8 R9 R10	R1 R2 R3 R4 R5 R6 R7 R8 R9 R10	R1 R2 R3 R4 R5 R6 R7 R8 R9 R10	R1 R2 R3 R4 R5 R6 R7 R8 R9 R10	R1 R2 R3 R4 R5 R6 R7 R8 R9 R10	R1 R2 R3 R4 R5 R6 R7 R8 R9 R10	R1 R2 R3 R4 R5 R6 R7 R8 R9 R10

Shoreface Dip Aligned Model

Grid Blocks / Layers	1200x400	600x200	300x100	240x80	120x40	60x20	30x10	24x8	12x4
24	Base		R1 R2 R3	R1 R2 R3	R1 R2 R3	R1 R2 R3	R1 R2 R3	R1 R2 R3	R1 R2 R3
12			R1 R2 R3	R1 R2 R3	R1 R2 R3	R1 R2 R3	R1 R2 R3	R1 R2 R3	R1 R2 R3
6			R1 R2 R3	R1 R2 R3	R1 R2 R3	R1 R2 R3	R1 R2 R3	R1 R2 R3	R1 R2 R3
3		R1 R2 R3 R4 R5 R6 R7 R8 R9 R10	R1 R2 R3 R4 R5 R6 R7 R8 R9 R10	R1 R2 R3 R4 R5 R6 R7 R8 R9 R10	R1 R2 R3 R4 R5 R6 R7 R8 R9 R10	R1 R2 R3 R4 R5 R6 R7 R8 R9 R10	R1 R2 R3 R4 R5 R6 R7 R8 R9 R10	R1 R2 R3 R4 R5 R6 R7 R8 R9 R10	R1 R2 R3 R4 R5 R6 R7 R8 R9 R10

Figure 6.2. Summary of the reservoir simulation carried out for each grid design

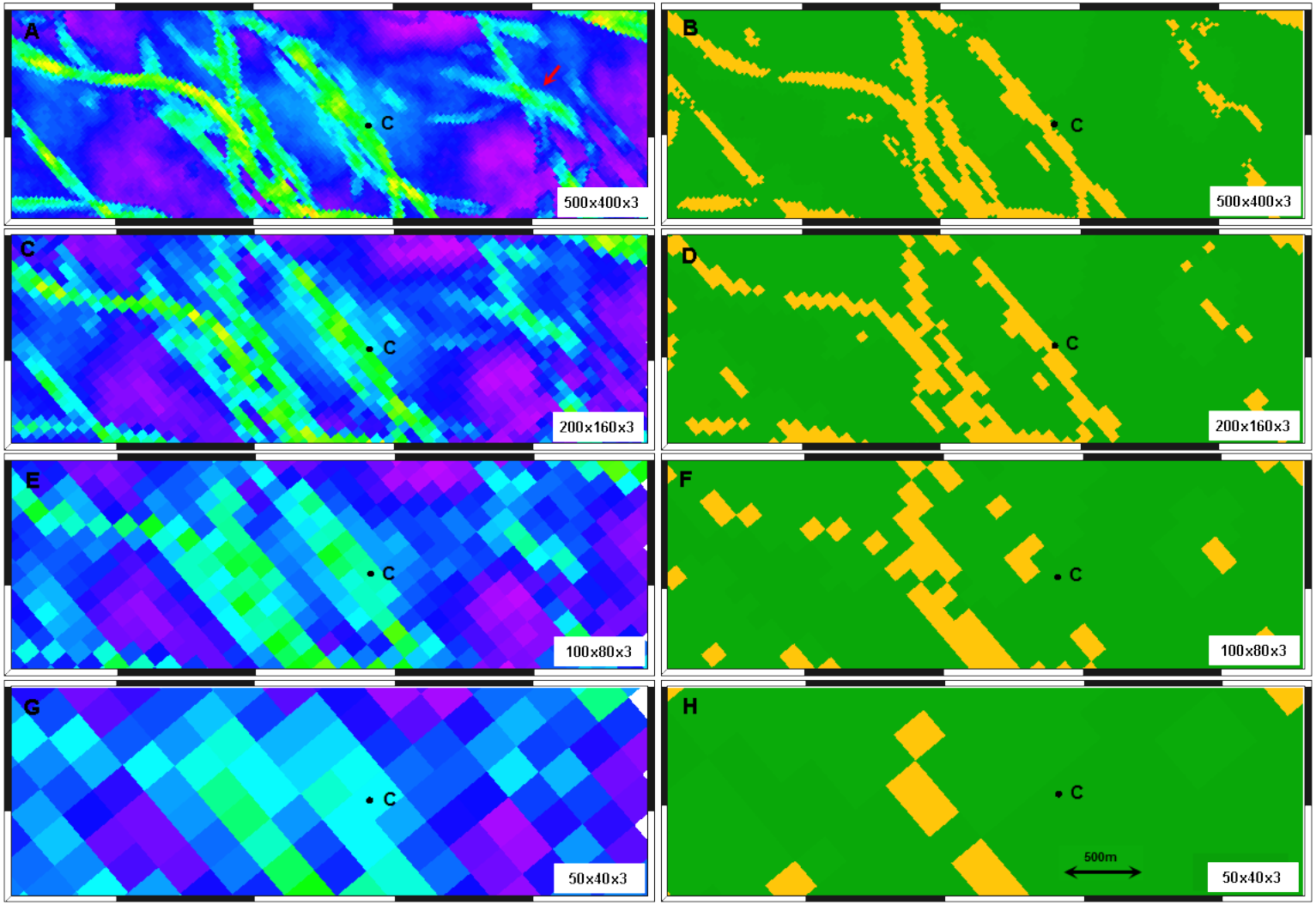

Figure 6.3. Upscaling porosity and channel facies. This figure highlights the different effects upscaling has on the porosity (left) and facies (right) models. The porosity associated with the channels near Well C remains in the model after it has disappeared from the facies model. The red arrow (A) highlights an area where channel properties remain even though the channels were lost due to vertical upscaling from 24 to 3 layers in the finest model.

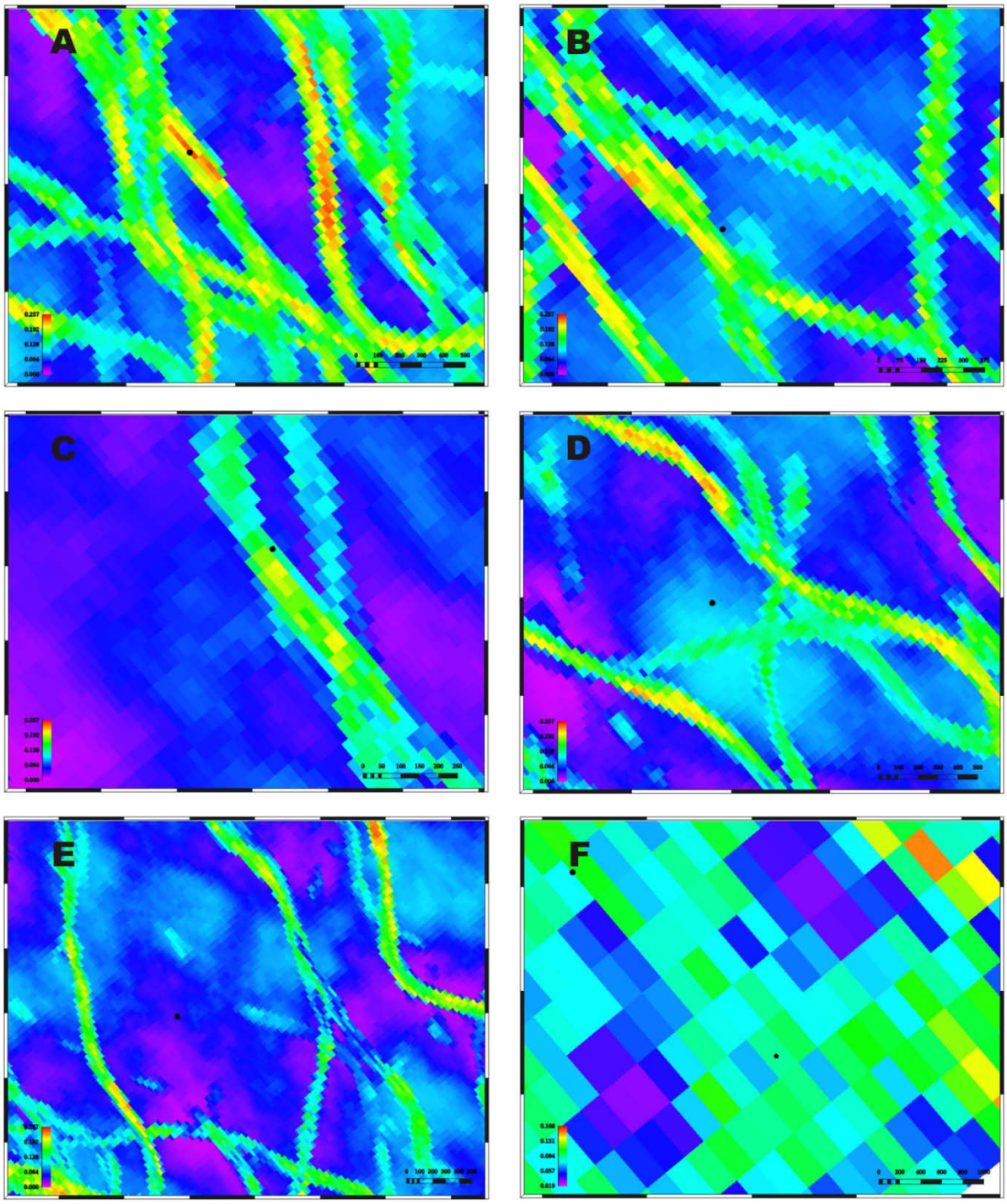

Figure 6.4. Samples of well position relative to porosity. Diagram A corresponds to code 6 (centre channel). Diagram B: code 3—outside channel edge; Diagram C: code 5—inside channel edge; Diagram D: code 2—overbank; Diagram E: code 1—floodplain, and Diagram F: code 4—bland.

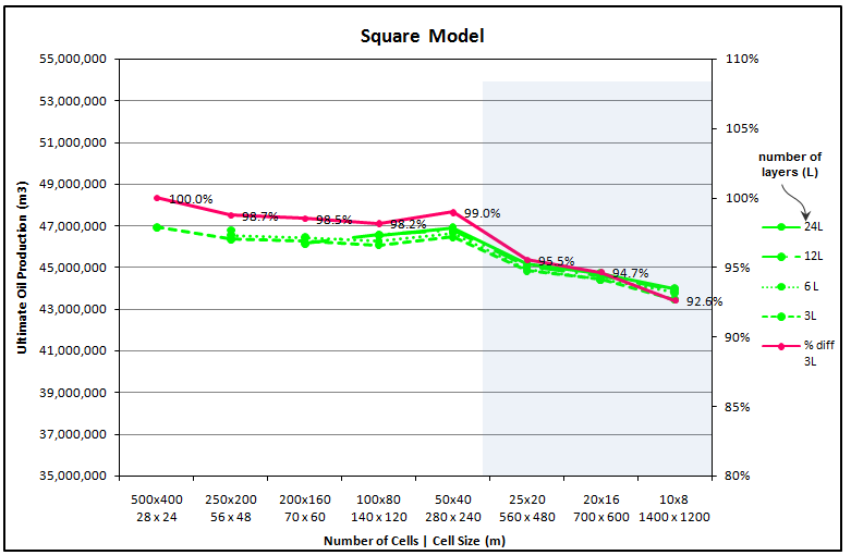

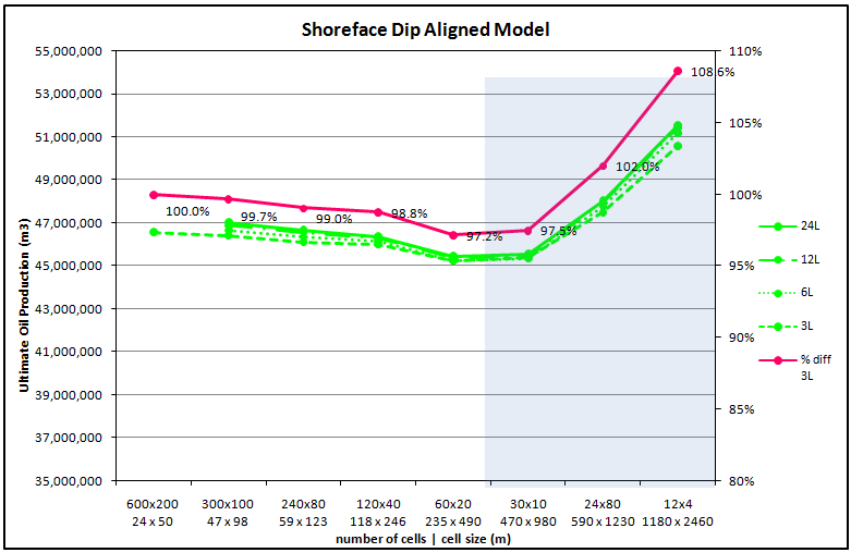

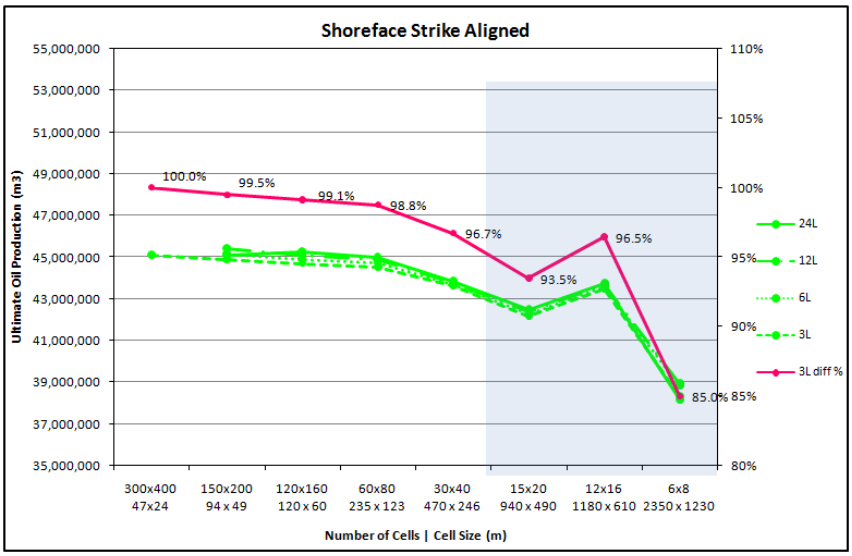

Figure 6.5. Ultimate Oil Production for the homogeneous model—all grid designs. This scenario consists of all cells having a porosity of 15% and a permeability of 1000 mD. This shows that the number of layers in the grid has little influence on the simulation results. The pink line indicates the percentage difference between the upscaled grid and the base model for the 3-layer grids. These indicate that for the grids with more than three cells between the injector and producers, the difference between the finest grid simulated and the upscaled grids is less than 5%. The square grid has the least change in total field production as a result of upscaling.

Grid Design	Rows	Columns	Multiplier	mX	mY	Number of Cells			
						24 layers	12 layers	6 layers	3 layers
Oblong	**600**	**800**	1	24	12	6,905,352			
	300	**400**	2	47	24	1,728,312	864,156	432,078	216,039
	150	**200**	4	94	49	432,984	216,492	108,246	54,123
	120	**160**	5	118	61	277,296	138,648	69,324	34,662
	60	**80**	10	235	123	69,600	34,800	17,400	8,700
	30	**40**	20	471	246	17,496	8,748	4,374	2,187
	15	**20**	40	942	491	4,392	2,196	1,098	549
	12	**16**	50	1177	614	2,784	1,392	696	348
	6	**8**	100	2354	1228	648	324	162	81
Square	**1000**	**800**	1	12	14	11,502,984			
	500	**400**	2	28	24	2,877,768	1,438,884	719,442	359,721
	250	**200**	4	56	48	720,384	360,192	180,096	90,048
	200	**160**	5	70	60	461,256	230,628	115,314	57,657
	100	**80**	10	140	120	115,632	57,816	28,908	14,454
	50	**40**	20	280	240	28,872	14,436	7,218	3,609
	25	**20**	40	560	480	7,320	3,660	1,830	915
	20	**16**	50	700	600	4,656	2,328	1,164	582
	10	**8**	100	1200	1400	1,128	564	282	141
Rectangle	**1200**	**400**	1	12	25	6,910,752			
	600	**200**	2	24	50	1,730,904	864,156	432,078	216,363
	300	**100**	4	47	98	433,872	216,936	108,468	54,234
	240	**80**	5	59	123	278,064	139,032	69,516	34,758
	120	**40**	10	118	246	69,972	34,896	17,448	8,724
	60	**20**	20	325	491	17,544	8,772	4,386	2,193
	30	**10**	40	471	982	4,392	2,196	1,098	549
	24	**8**	50	588	1228	2,784	1,392	696	348
	12	**4**	100	1177	2456	696	348	174	87

Figure 6.6. Grid dimensions and number of cells.

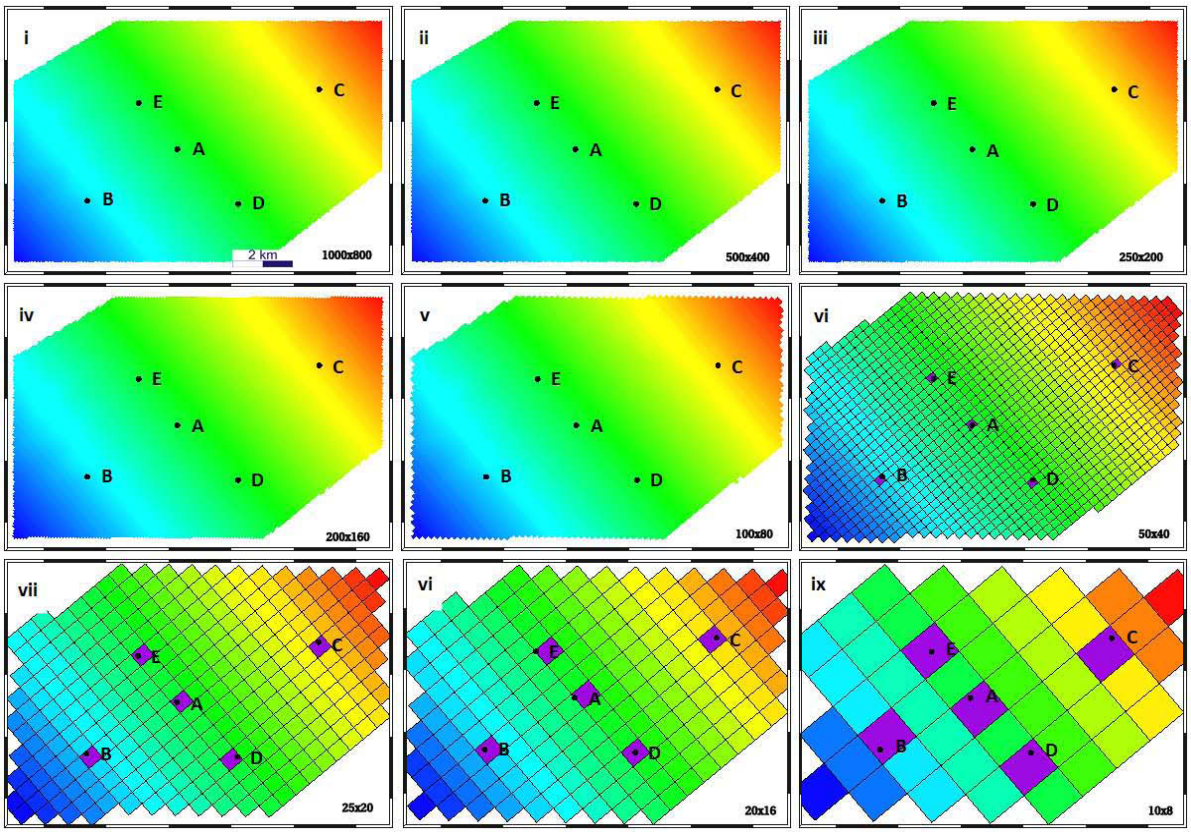

Figure 6.7. Cell design for the Square grid, showing location of the 5 vertical wells (A,B,C,D,E). The purple cells are the blocked wells for each grid (i.e. they show which column the well is modelled in for that grid). Well A is the injector in all reservoir simulation. Figure vii indicates that upscaling to 25 x 20 cells or fewer introduces potential errors in results due to insufficient cells between wells. The grid is rainbow coloured to aid identification of increasing cell size, and do not reflect the model structure or cell content.

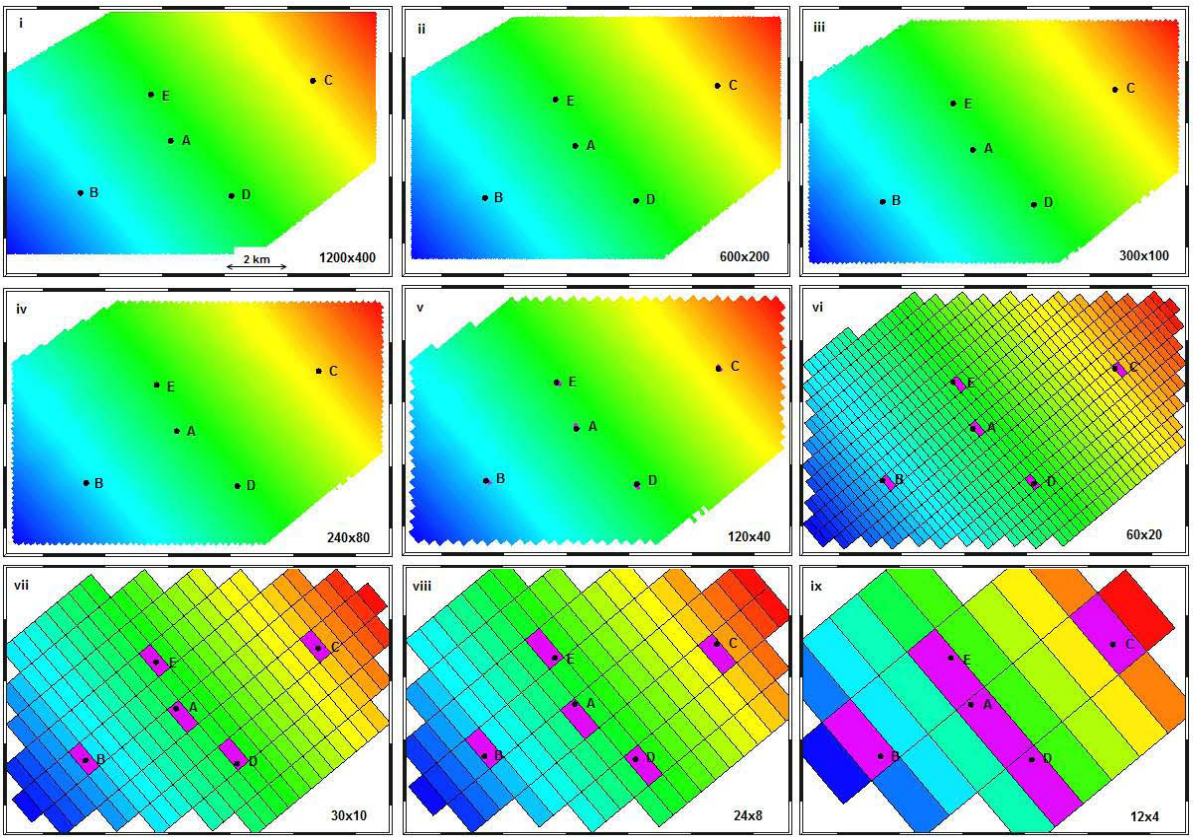

Figure 6.8. Cell design for the SDA grid, showing location of the 5 vertical wells (A,B,C,D,E). The purple cells are the blocked wells for each grid (i.e. they show which column the well is modelled in for that grid). Well A is the injector in all reservoir simulation. Figure vi indicates that upscaling to 60 x 20 cells or fewer introduces potential errors in results due to insufficient cells between wells. The grid is rainbow coloured to aid identification of increasing cell size, and do not reflect the model structure or cell content.

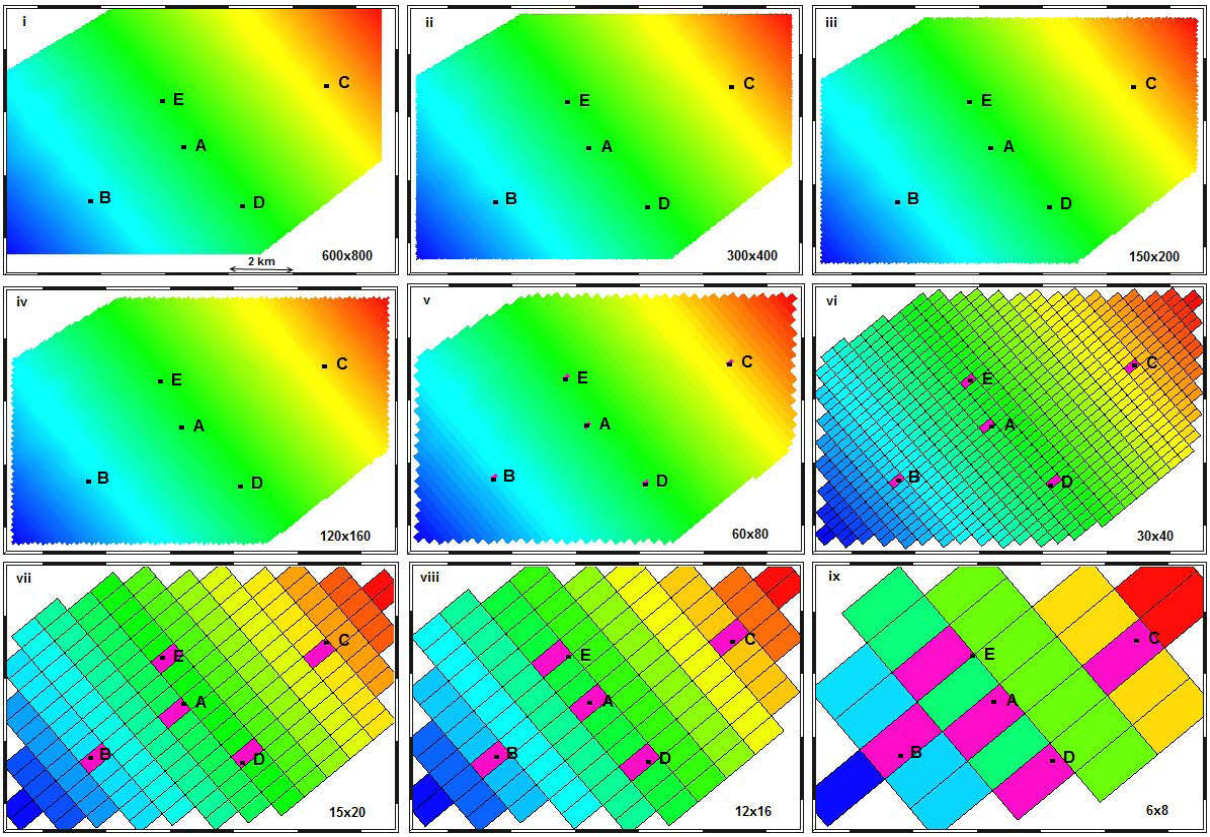

Figure 6.9 Cell design for the SSA grid, showing location of the 5 vertical wells (A,B,C,D,E). The purple cells are the blocked wells for each grid (i.e. they show which column the well is modelled in for that grid). Well A is the injector in all reservoir simulation. Figure vii indicates that upscaling to 15 x 20 cells or fewer introduces potential errors in results due to insufficient cells between wells. The grid is rainbow coloured to aid identification of increasing cell size, and do not reflect the model structure or cell content.

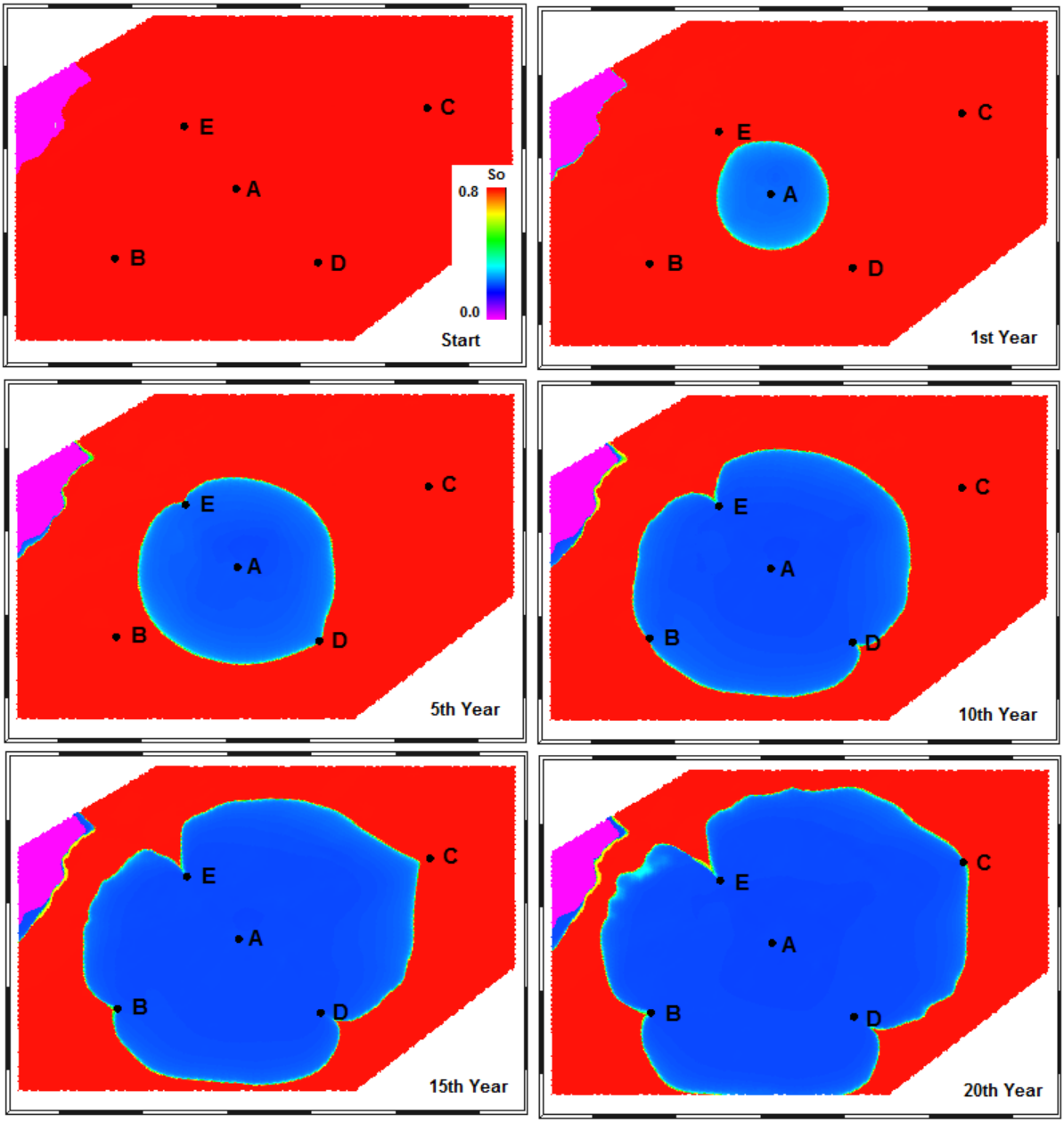

Figure 6.10. Water influx into homogeneous model. 500 x 400 x 3 SQ grid. The water influx during the early stages of production has a radial distribution. The influence of the structure is apparent on the edge of the water influx between wells B and E in the 15th and 20th years. Water reaches wells D and E at approximately the same time (in the second year), followed by Well B. Well C is the last well to experience water breakthrough.

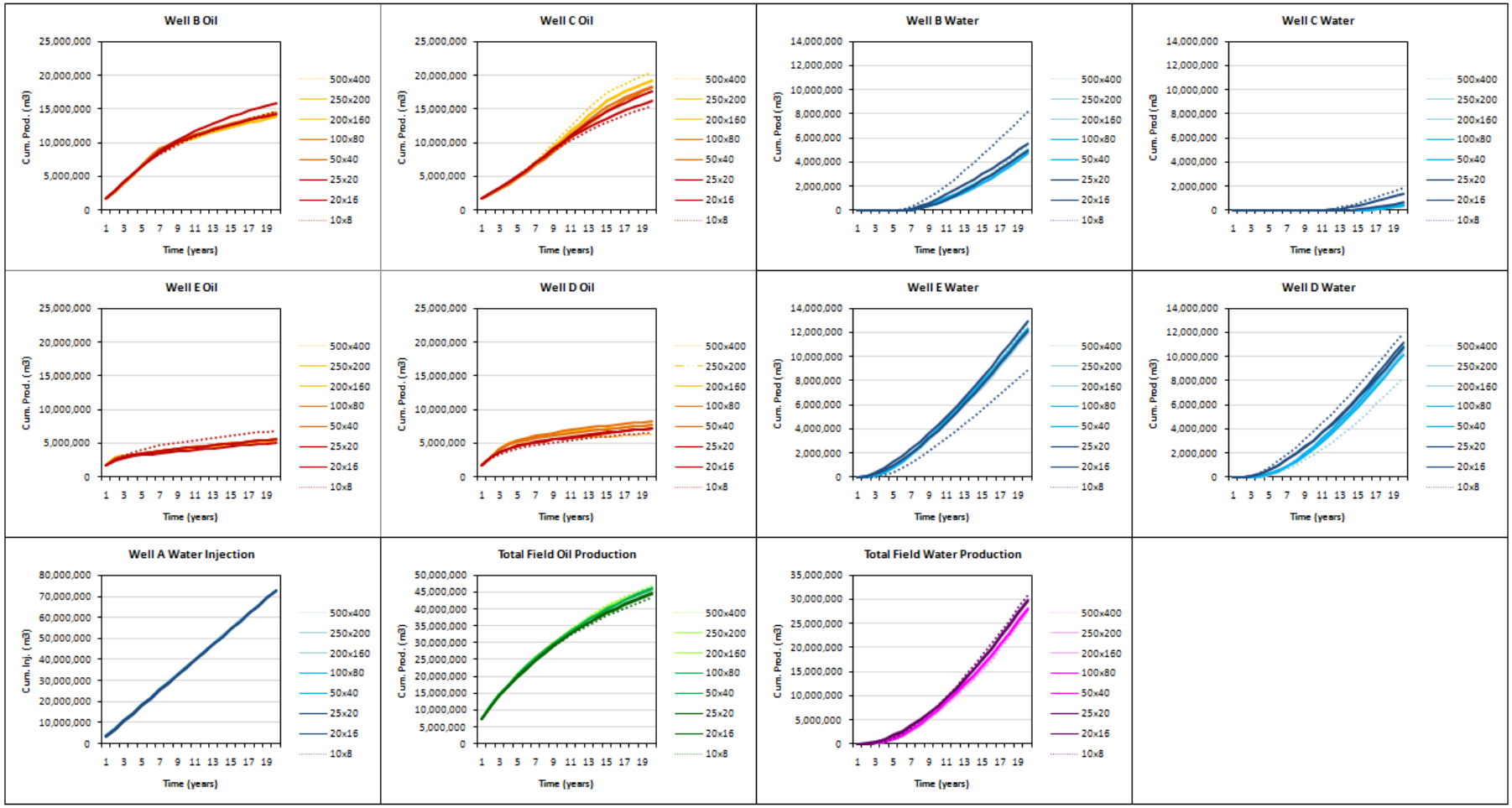

Figure 6.11. Cumulative recovery by well. Square grid, homogeneous model. This figure shows the differences in production behaviour of the four wells in a homogeneous model. As shown in Figure 6.10, wells B and C, which are furthest from the injector experience water break though later than wells D and E. Wells B and C recover more oil than wells D and E. As wells D and E experience early water break though their production rapidly tapers off. The 10 x 8 grid has a very different pattern of water recovery from the other grids, highlighting the unreliability of this grid. Well C, which experiences water break though last, has the most variation in oil recovery between the grids. However, this difference is negated by the variability in the other wells, and does not have a major influence on the total field recovery.

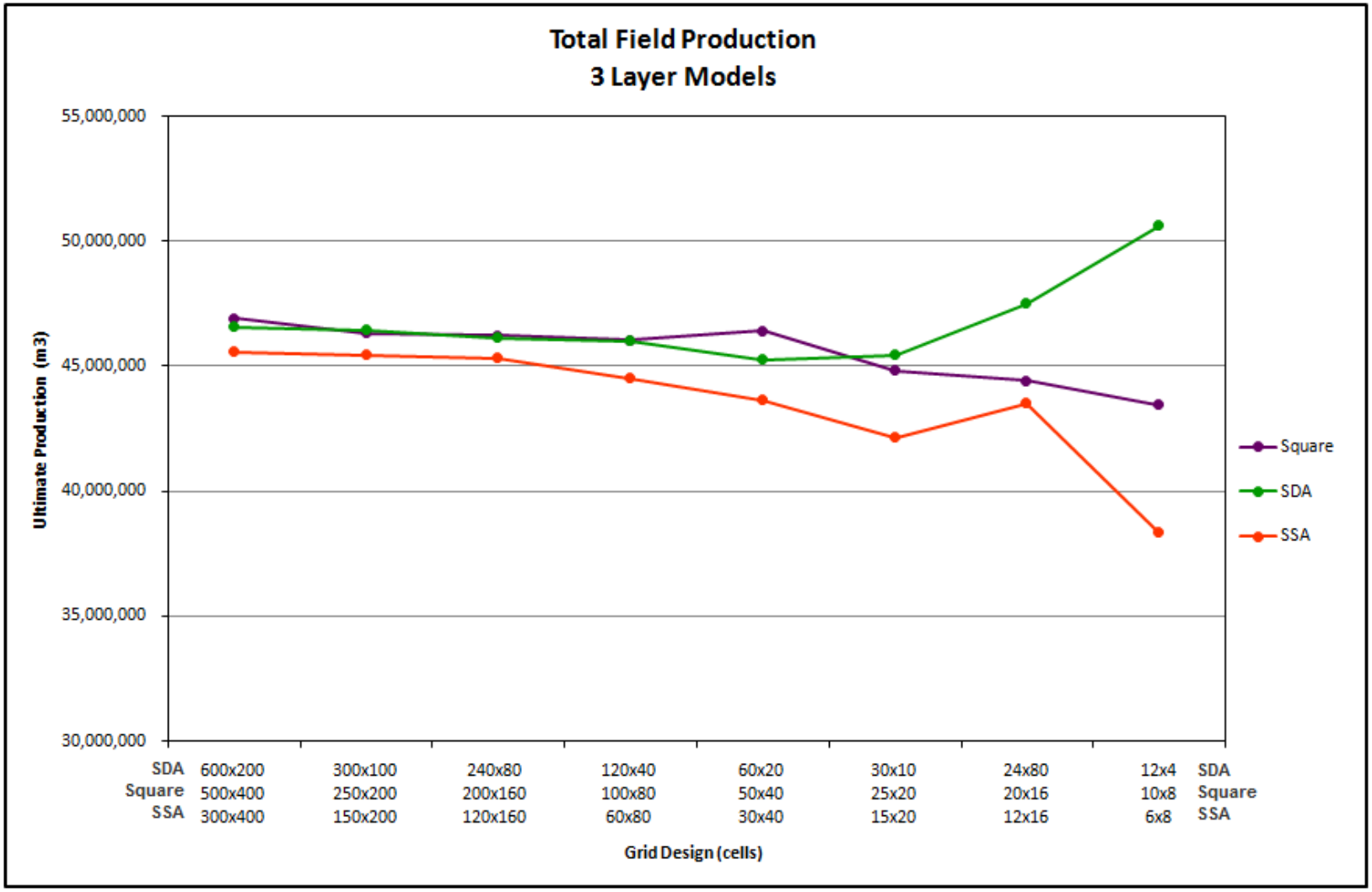

Figure 6.12. A comparison of the ultimate field production of the 3-layer grids with different grid designs. The models are compared at equivalent amounts of upscaling from their original grids. This allows comparison at similar cell dimensions. For example, the cells in the SDA600 x 200 grid are 24x50 m, while the cells in the square 500 x 400 grid are 28x24m, and the cells in the SSA 300 x 400 grid are 47x24m.

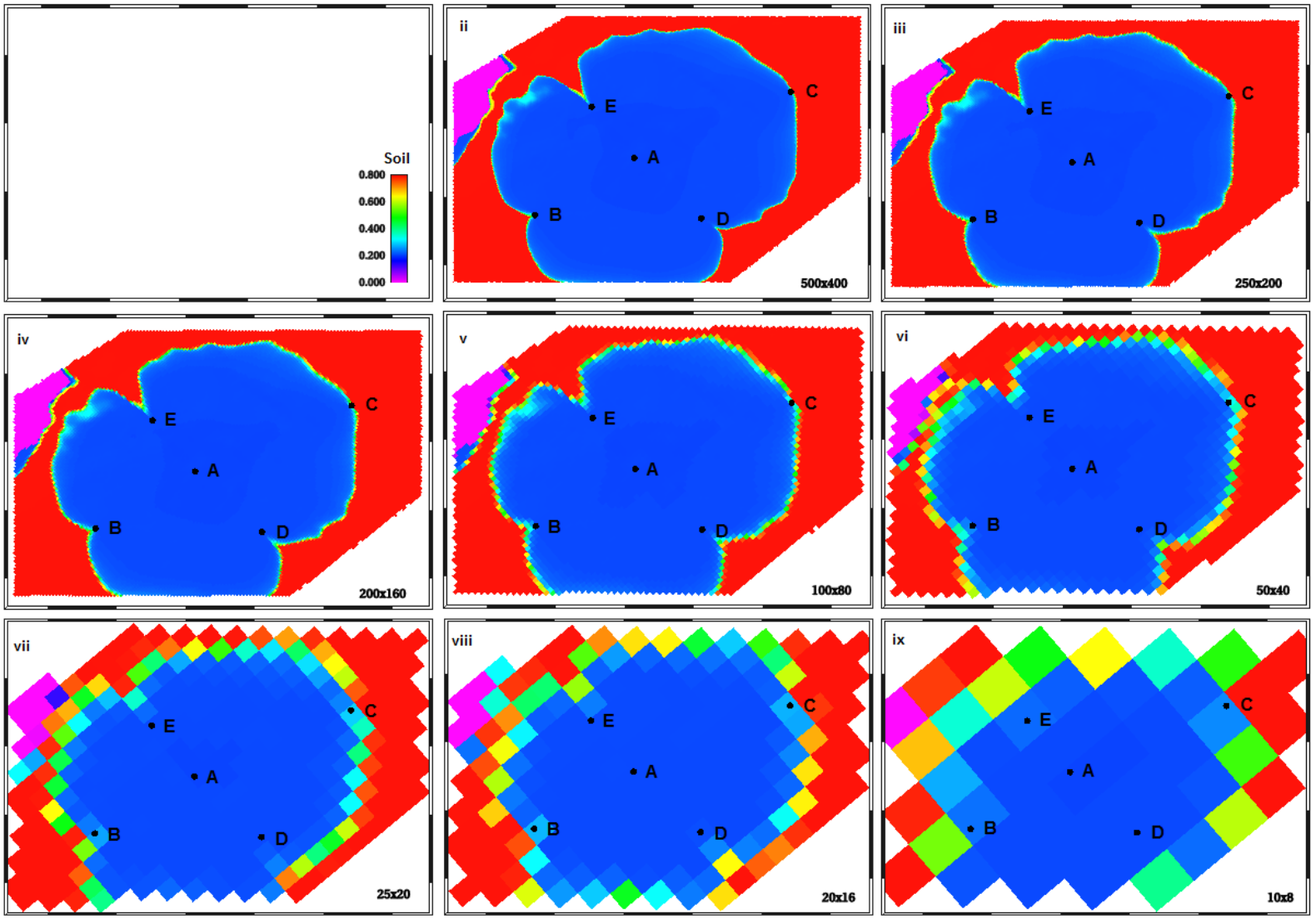

Figure 6.13. Square grid homogenous grid. Simulation at 20 years, layer 3 of model (base). The production and injection rates and pressures were designed so that all wells would be producing some water at the end of 20 years production.

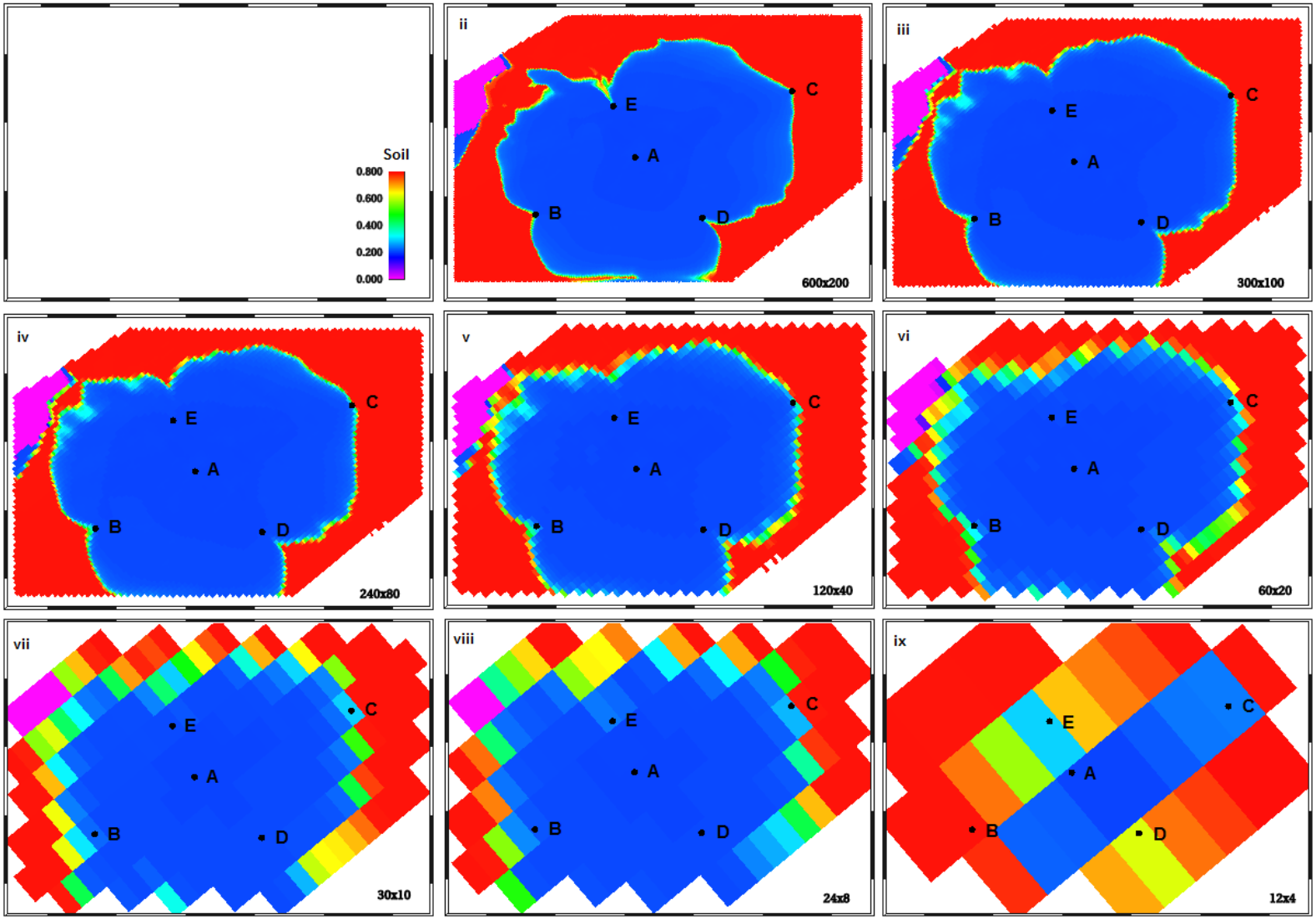

Figure 6.14. SDA grid, homogeneous model. Reservoir simulation results at the end of 20 years production, layer 3 of model (base).

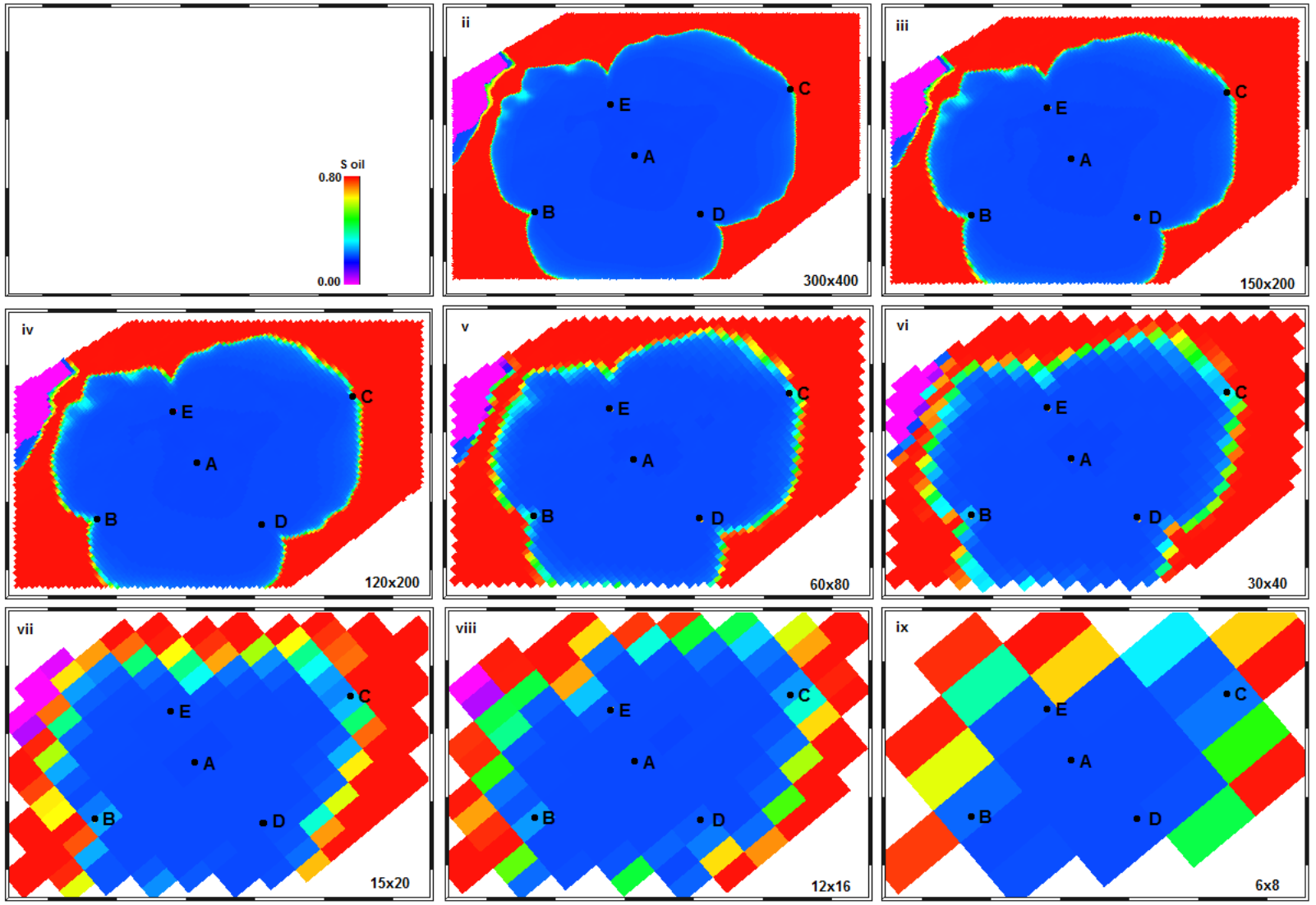

Figure 6.15. Results of reservoir simulation of homogeneous model at the end of 20 years production. SSA grid, 3-layer grid. Base layer of model.

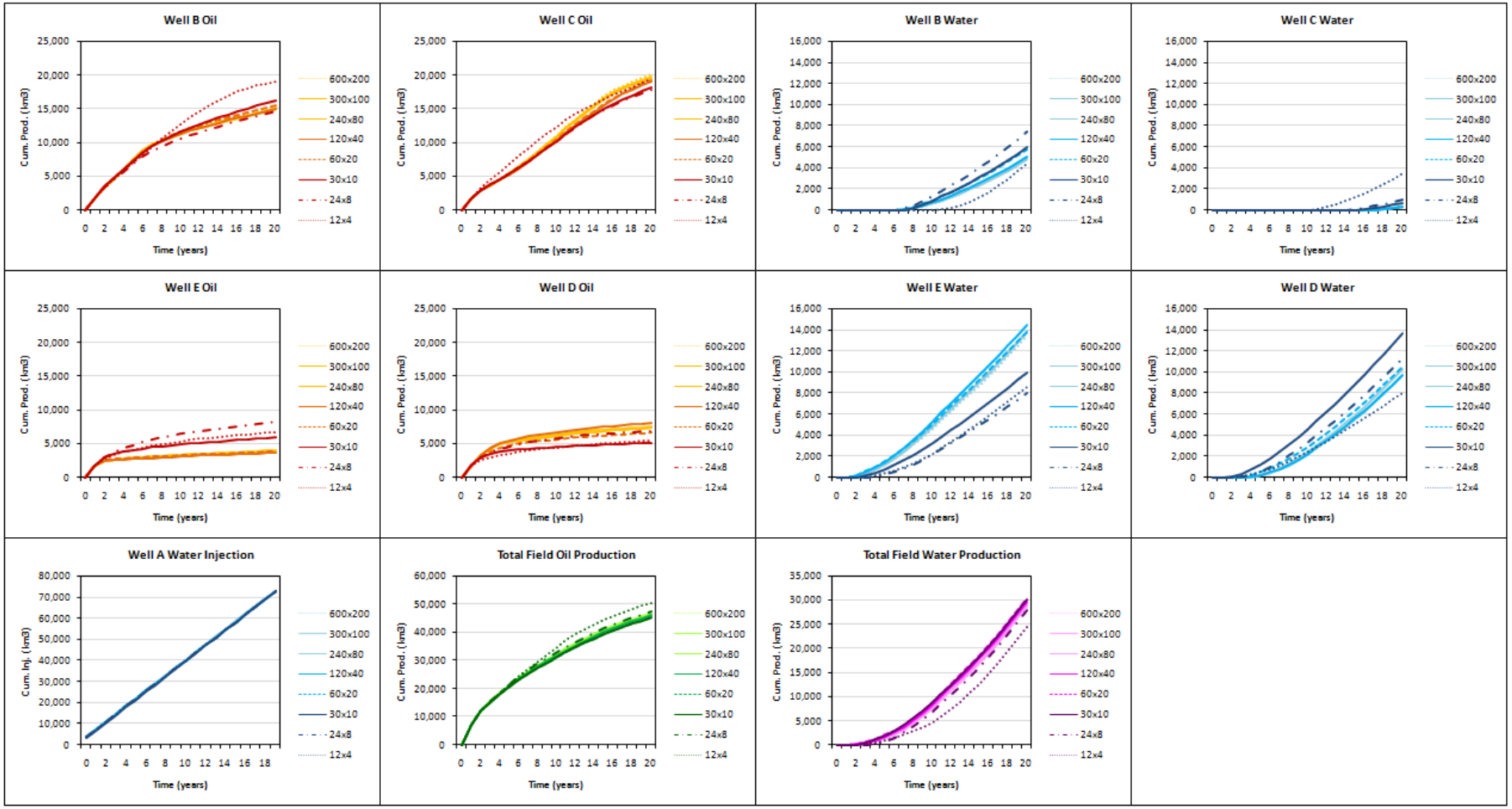

Figure 6.16. Individual well production from the homogeneous 3 layer SDA grid. Like the square grid, the SDA grid shows early water breakthrough in wells D and E, and later breakthrough, and corresponding higher oil production in wells B and C. Also of note is that the 60 x 20 grid has a very similar production profile to the 120 x 40 grid. There are only three cells between the injector (well A) and well E (Figure 6.8). The production profiles for well E show a clear difference in behaviour between the 60 x 20 grid and the 30 x 10 grid. In all grids except the 12x4 grid there are more than three cells between well A and wells B and C.

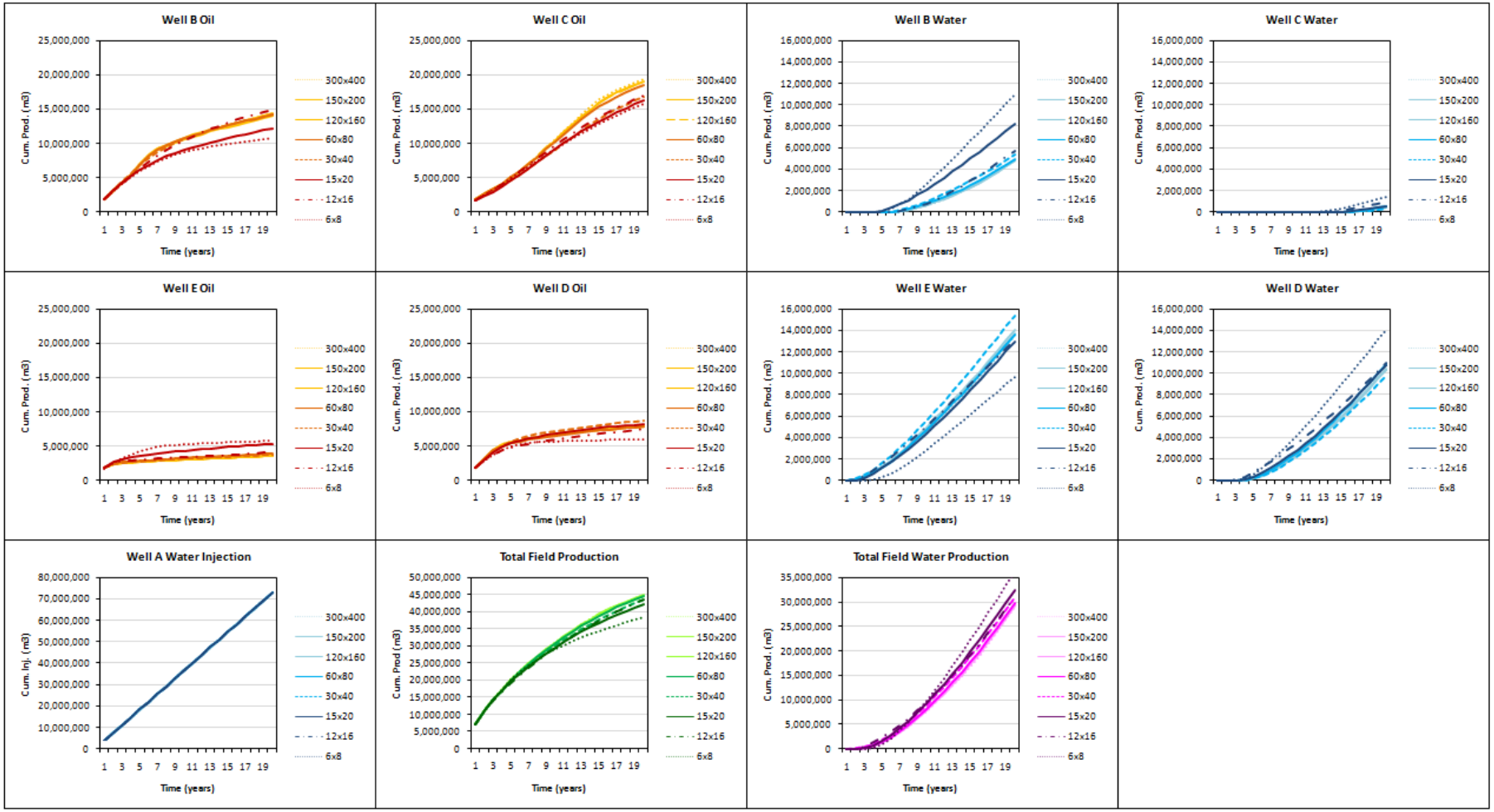

Figure 6.17. Individual well production from the homogeneous 3 layer SSA grid. These graphs show that there is a change in the behaviour of all wells between the 30 x 40 grid and the 15 x 20 grid. This corresponds to the point at which there are three cells or fewer between the injector and several of the producers. The difference is subtle of the total field production.

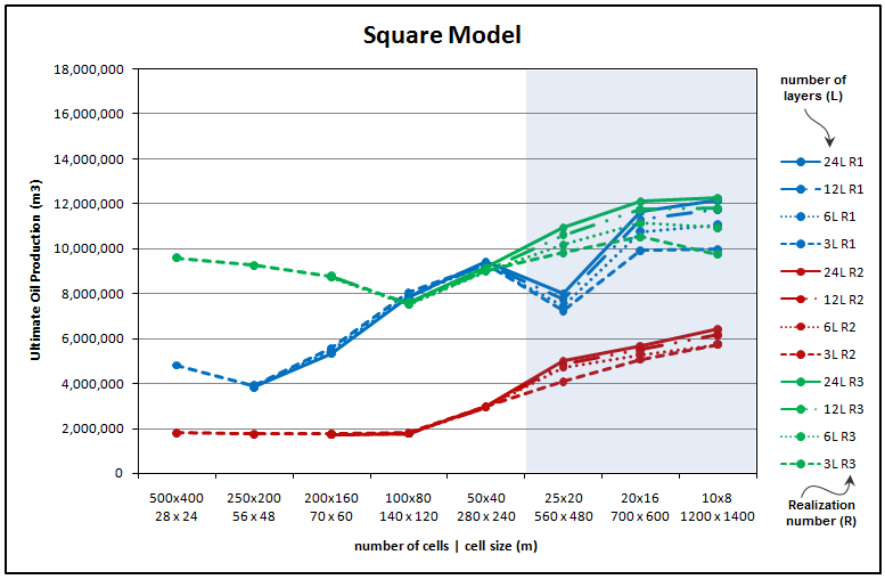

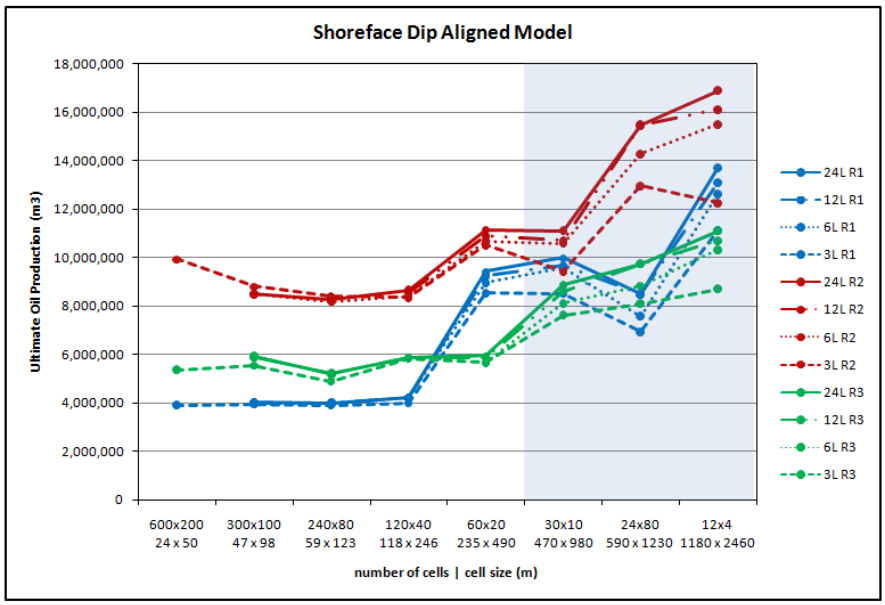

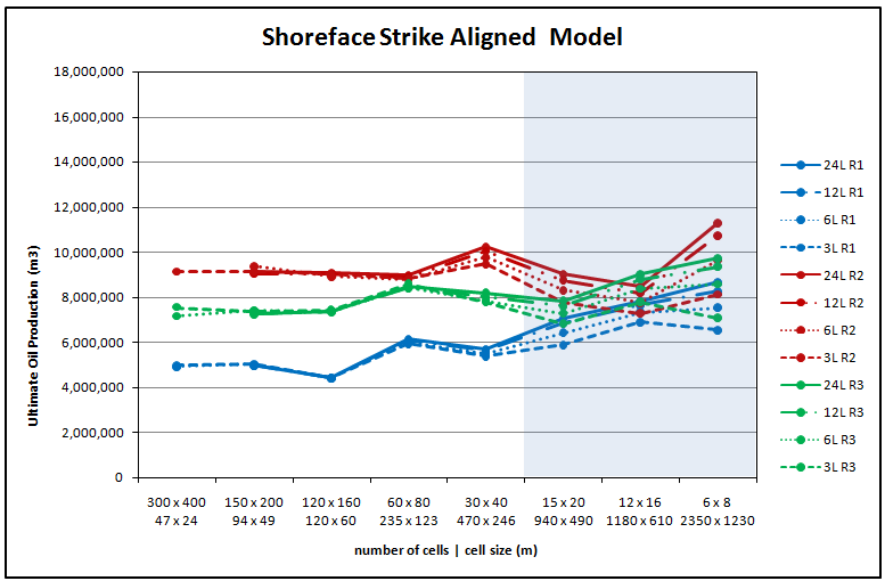

Figure 6.18. A comparison of simulation results for vertical and horizontal upscaling. 100-25 scenario. For all three grid designs, vertical upscaling does not result in a significant change in ultimate field recovery until there are three cells or fewer between the injector and at least one producing well in the field (area of blue-grey tint). See *Appendix 5* for examples of other scenarios.

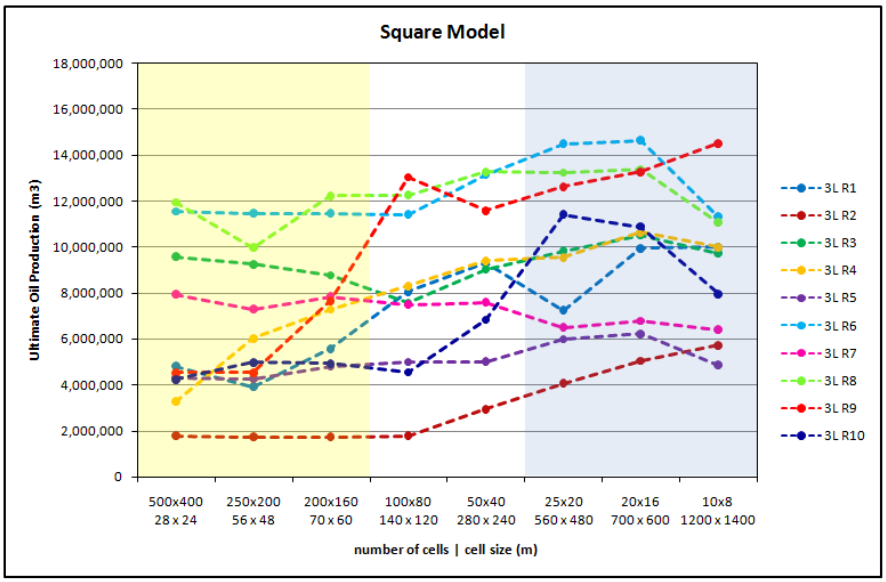

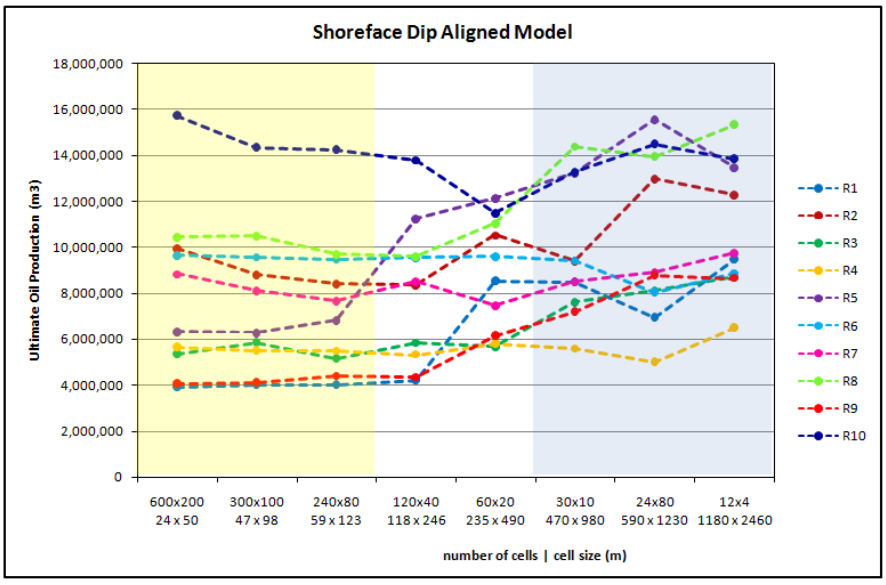

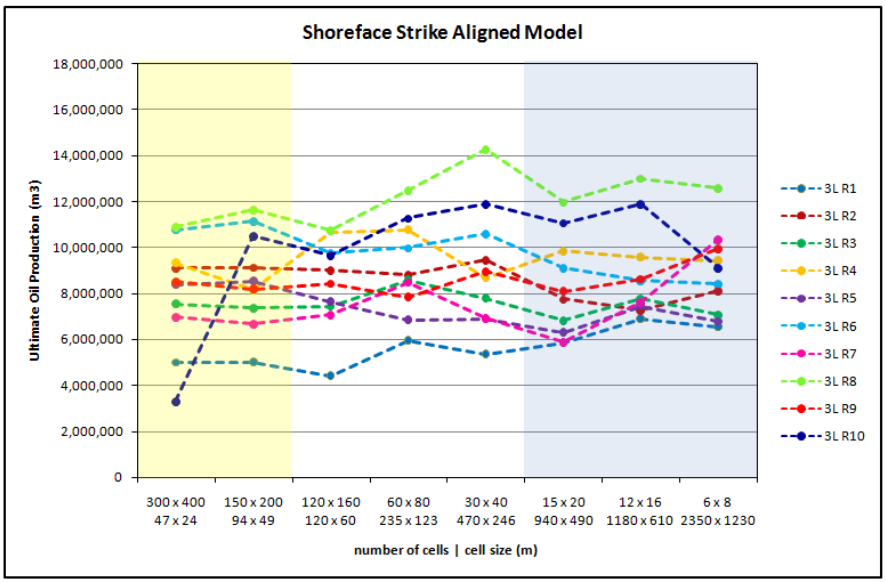

Figure 6.19. Total field production for the 100-25 scenario. Grids where grid cells are smaller than channel width are highlighted by the yellow tint. The blue-grey tint highlights grids where there are three or fewer cells between the injector and at least one of the producers. For all the grid designs there is a difference in ultimate oil production between the realizations of $8x10^6$ to $12x10^6$ cubic metres.

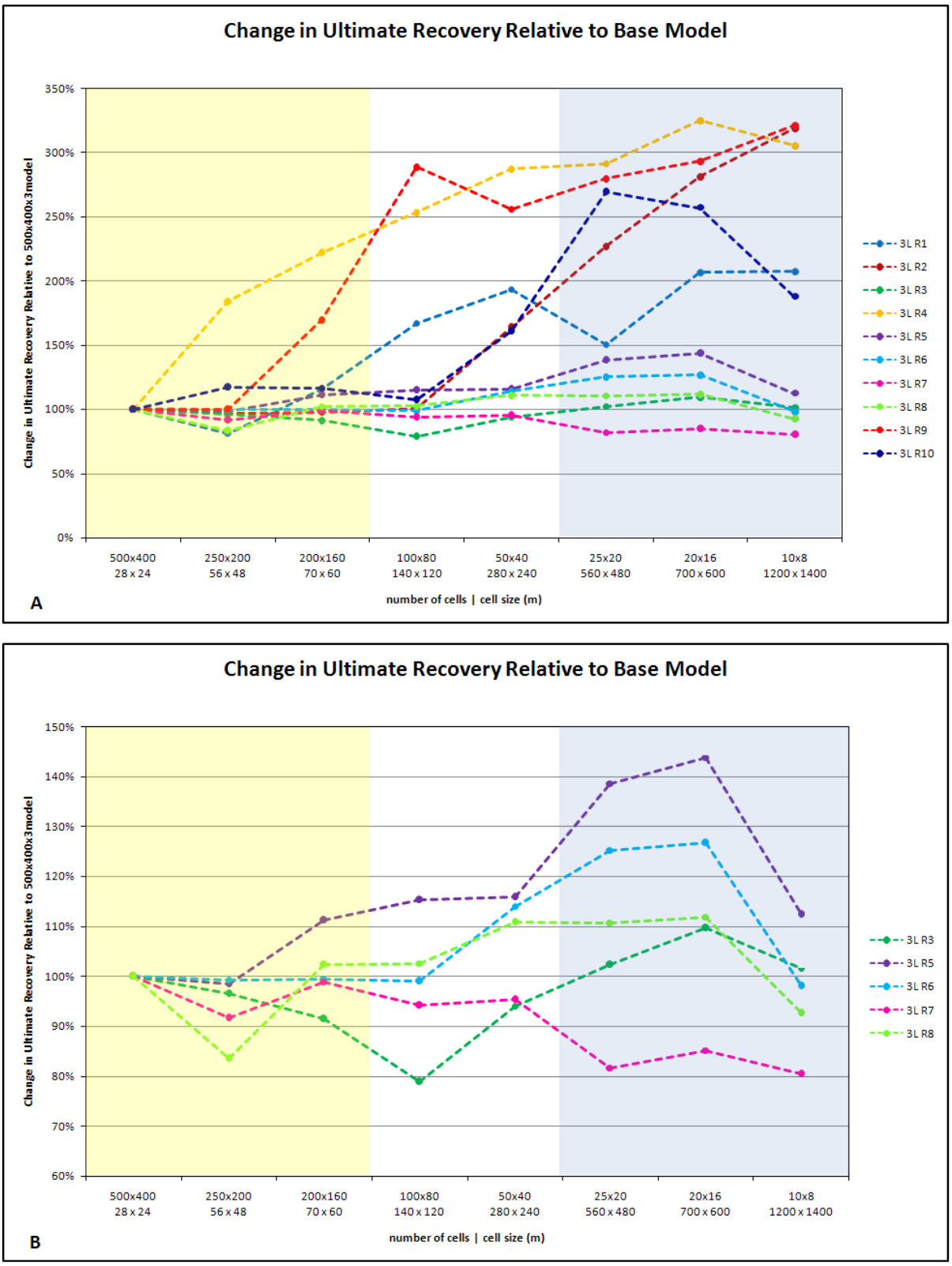

Figure 6.20. Change in ultimate recovery, SQ100-25 scenario, 3 layers. These charts show the percentage difference in ultimate oil production between the finest grid modelled (500 x 400) and subsequent grid designs. Chart A highlights the realizations where the difference between the finest grid modelled and the coarsest grid modelled is between 150 to 300%. Chart B shows that even the realizations that appear to have minor change in results in Chart A, actually show similar trends when realizations with large magnitude changes are removed from the chart.

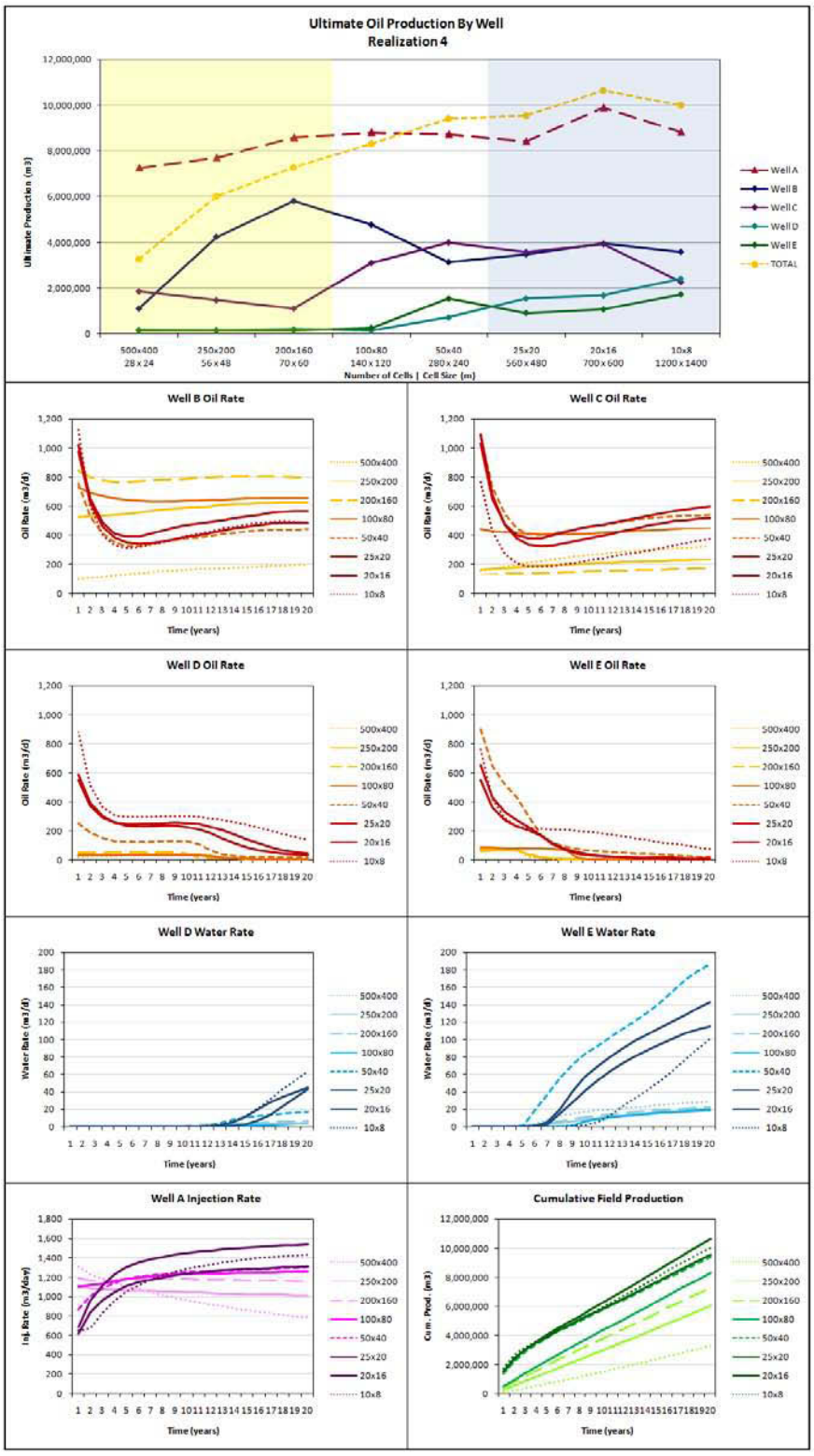

Figure 6.21. Production characteristics of Realization 4 SQ100-25 scenario. The top diagram shows the ultimate recovery by field (yellow line) and by well. The red line shows the total amount of water injected into Well A. The smaller charts show the oil and water rates for the wells. No water was produced from Wells B and C. These plots indicate that the rate, and decline patterns for all wells change significantly between the 100 x 80 grid and the 50 x 40 grid. Although the 100 x 80 grid has a oil rate decline pattern similar to the 200 x 160 grid in wells B and C, its rate and ultimate recovery do not follow the trend set by the finer grids. The changes in behaviour occur at the point at which the cells become larger than the channel width and at the point at which the porosity distribution switches from bimodal to normal. Visually, this is the point at which the porosity grid begins to look bland.

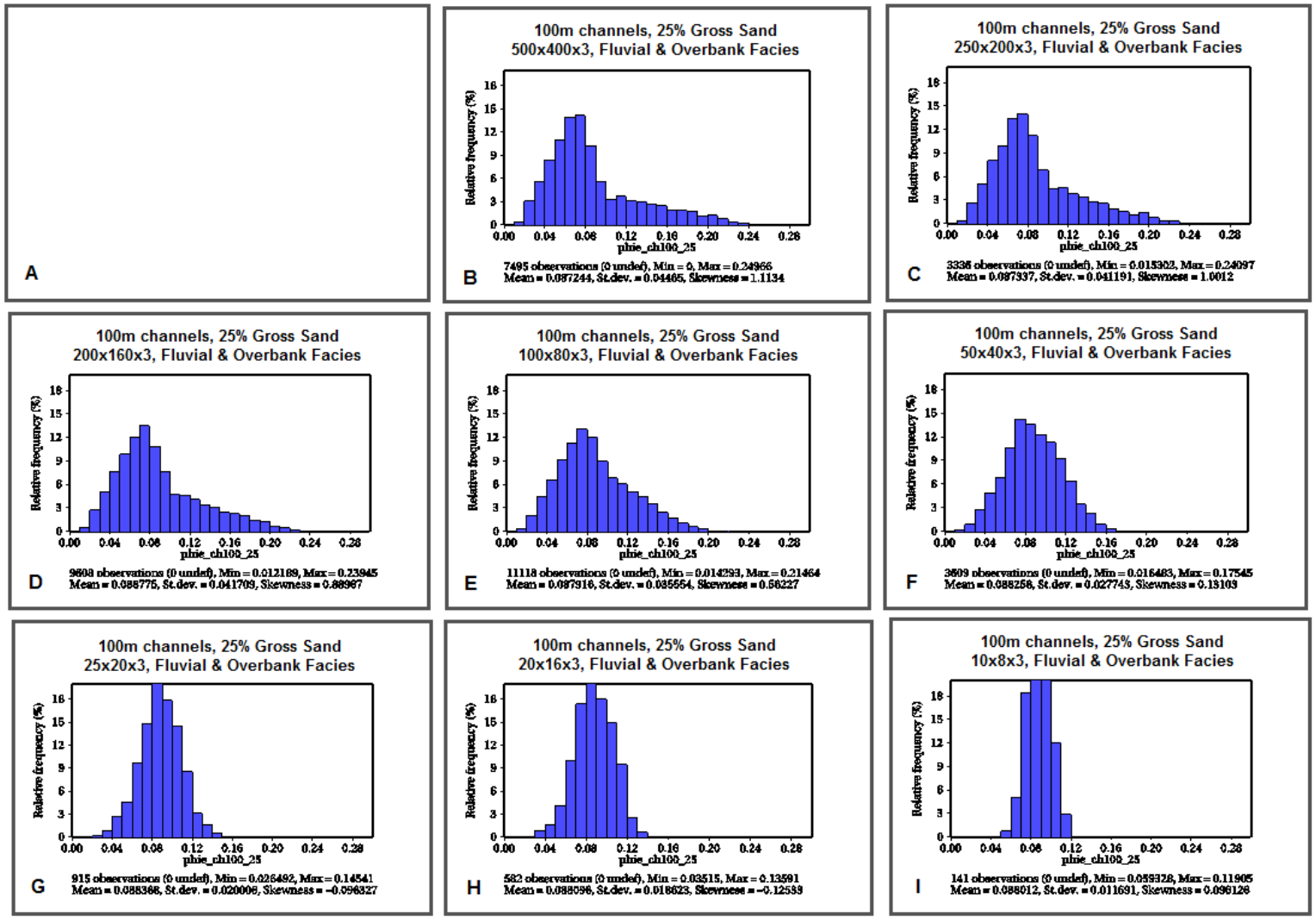

Figure 6.22. Porosity distribution, SQ100-25 scenario. Realization 4. The channel width is exceeded by the cell width in the 100 x 80 x 3 grid (E). The porosity distribution for this grid is closer to that of the smaller grids (B,C &D) than to that of the larger grids. The shift in porosity distribution from skewed to approximately normal occurs in the 50 x 40 x 3 grid (F). This is the point that the porosity models begin to appear 'bland' (see Figure 6.23 and Figure 6.5).

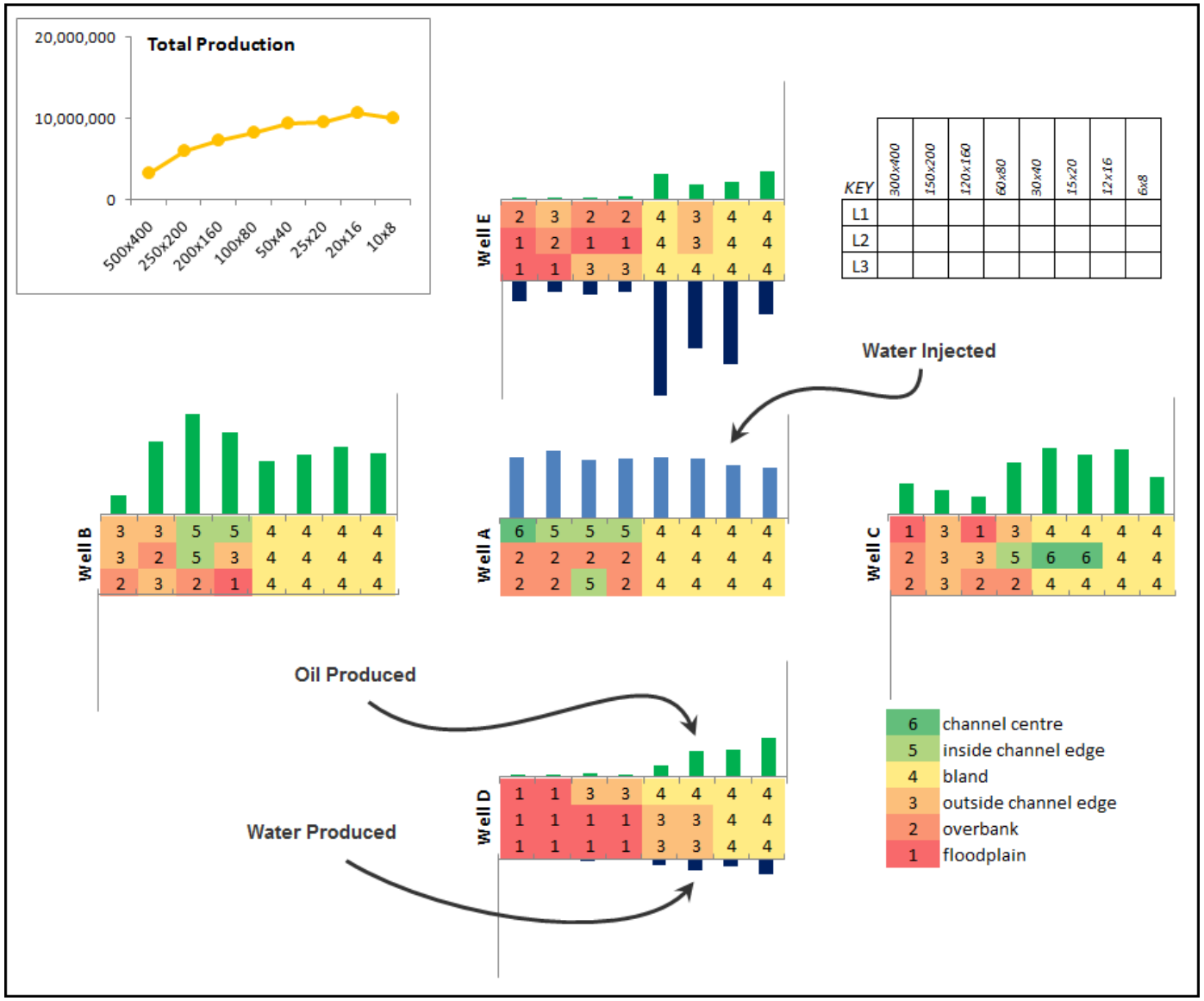

Figure 6.23. Channel proximity to wells. Realization 4, SQ100-25 scenario. This diagram captures a visual estimate of the position of the wells relative to porosity associated with channels. Wells are arranged in the pattern in which they are distributed in the model. Green cells denote that the well is located near the centre of a channel. Pale green and orange, indicate that the well is close to a channel edge, red that they are not close to a channel, in an area of very low porosity. Yellow cells indicate that the porosity distribution is 'bland' and that no channels are identifiable. The bar charts show the ultimate recovery or injection of the well. The scale for the green bars is the same for all wells, and the blue bars also have matching scales. The injector well (A) penetrates the centre of a channel in one layer and the amount of injection is relatively constant for all grids. Wells D and E, both of which have poor production (Figure 6.21) are not close to any channels. Production in these wells improves when the grids are upscaled to a level where the porosity distribution becomes 'bland' (50 x 40 grid). Wells B and C are located close to a channel. As the grids are upscaled Wells B and C go from being on the outside edge of a channel (low porosity) to the inside edge (good porosity). As this occurs there is an increase in production from the wells.

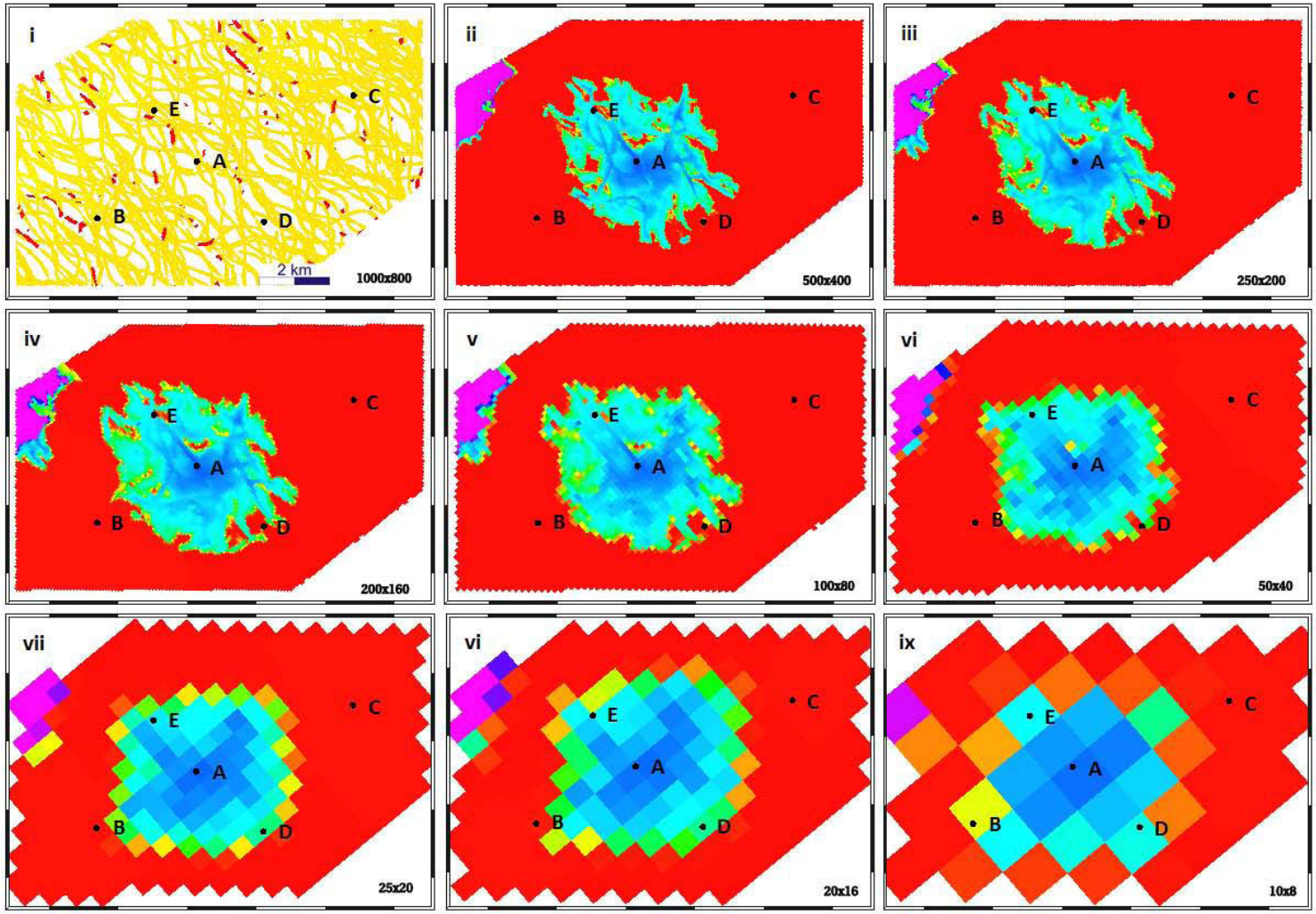

Figure 6.24. Oil Saturation. Water injection patterns at the end of 20 years. SQ100-25 scenario, Realization 4, layer 3 of 3. Figure i shows the connectivity of channels of the original 1000 x 800 x 24 facies model. There are multiple channels in the vicinity of Well A, allowing for water influx in all directions. Note the blurring of the water flow along the channels as the cells get larger. Channel width is approximately the same as the cell width in the 100 x 80 grid.

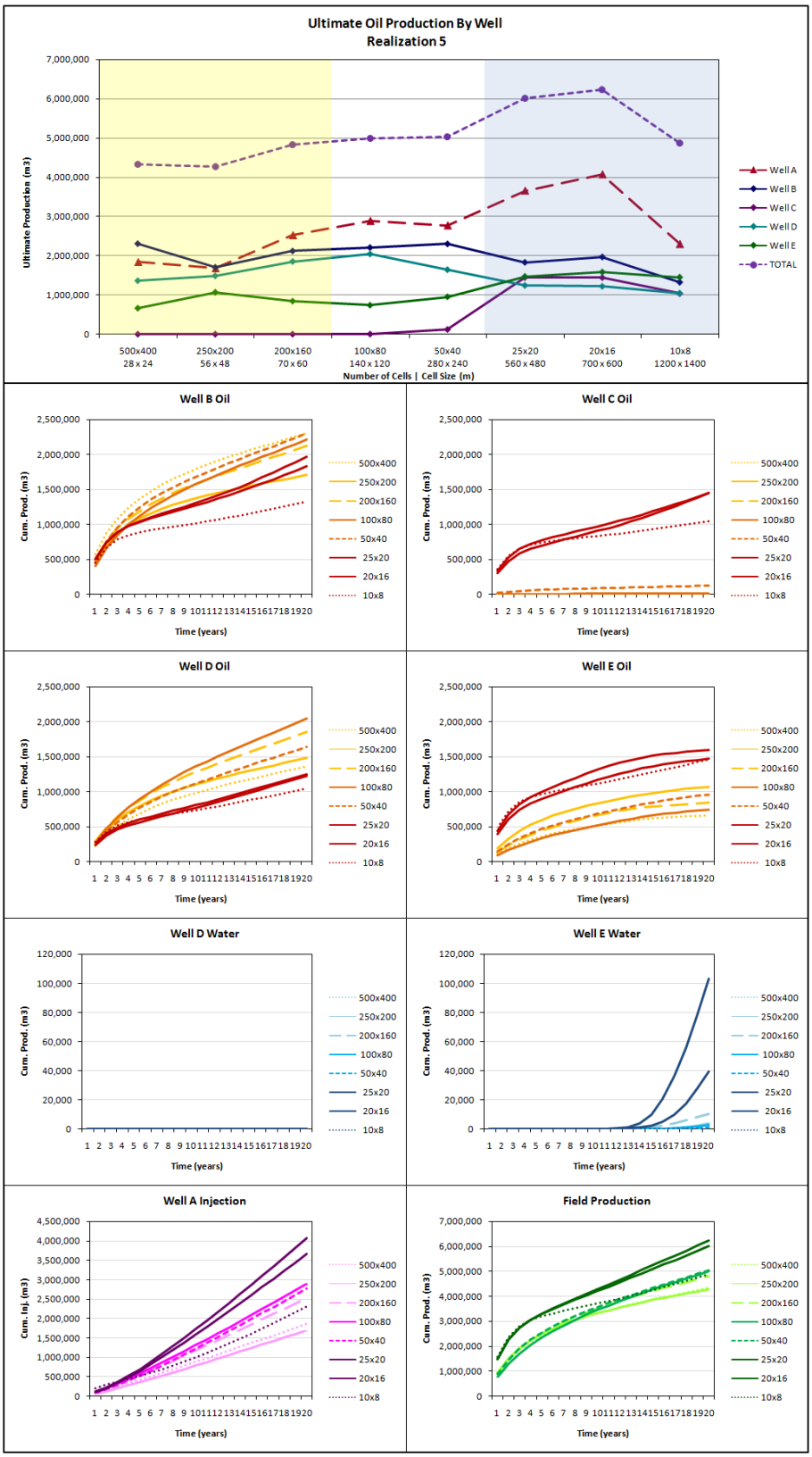

Figure 6.25. Cumulative oil and water production for SQ100-25 scenario, Realization 5. Compared to other realizations, the changes in cumulative production as cell size increases are small. Well C does not penetrate any channels (Figure 6.26) and does not contribute to the production until the cell size is larger than the channel width. There are subtle changes in the trend of the ultimate recovery graph (top) for Wells A and B between the 250 x 200 and 200 x 160 grids.

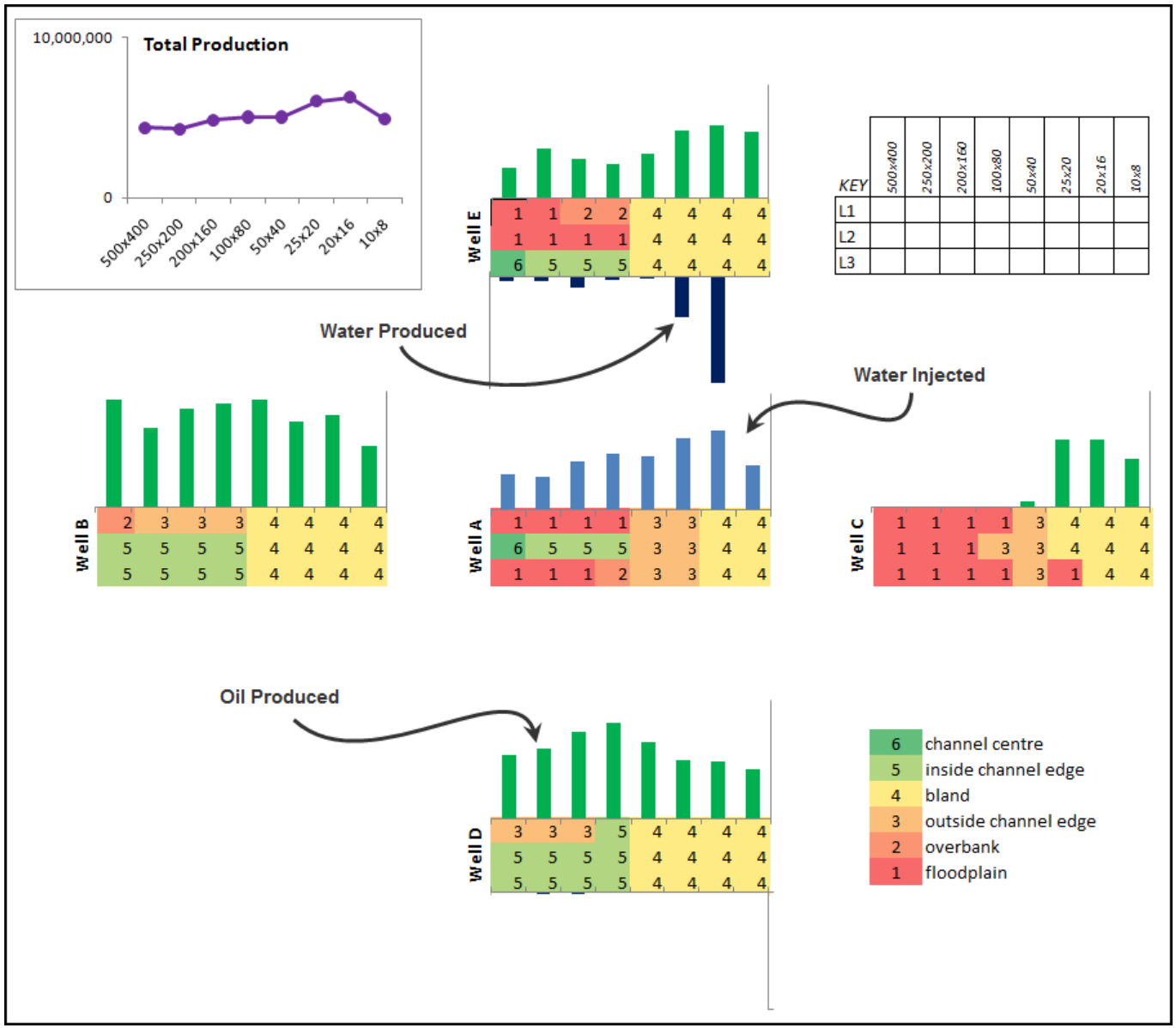

Figure 6.26. Channel proximity to wells. Realization 5, SQ100-25 scenario. The total production is relatively consistent for all grids. Most wells in this realization penetrate a channel in at least one layer.

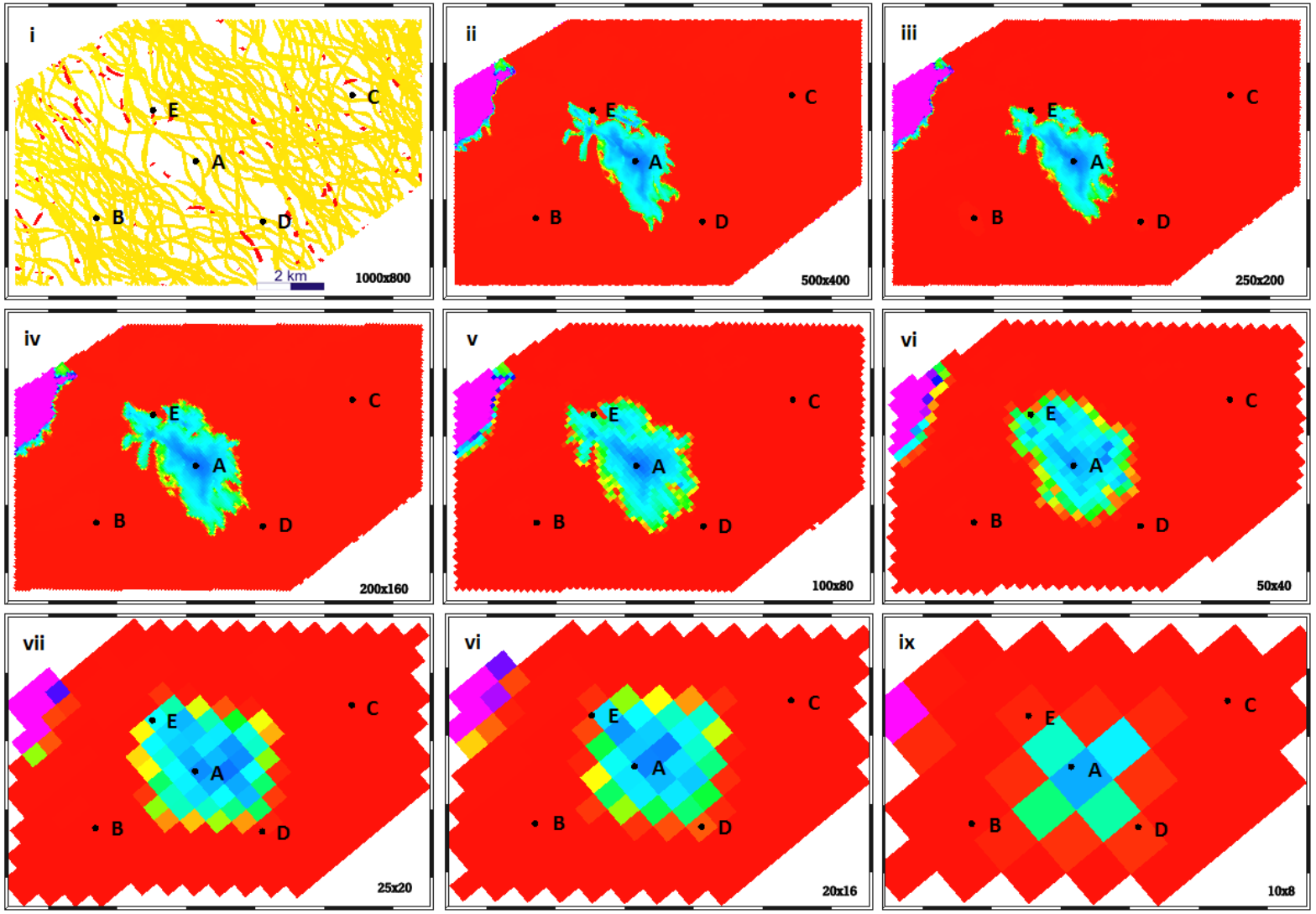

Figure 6.27. Oil Saturation. Water inflow at the end of 20 years, SQ100-25 scenario, Realization 5, Layer 3 of 3. Figure i shows the channel connectivity for all layers 3 in the original 1000 x 800 x 24 grid. This indicates there are few channels in the vicinity of Well A. The water influx appears to be following the orientation of these channels.

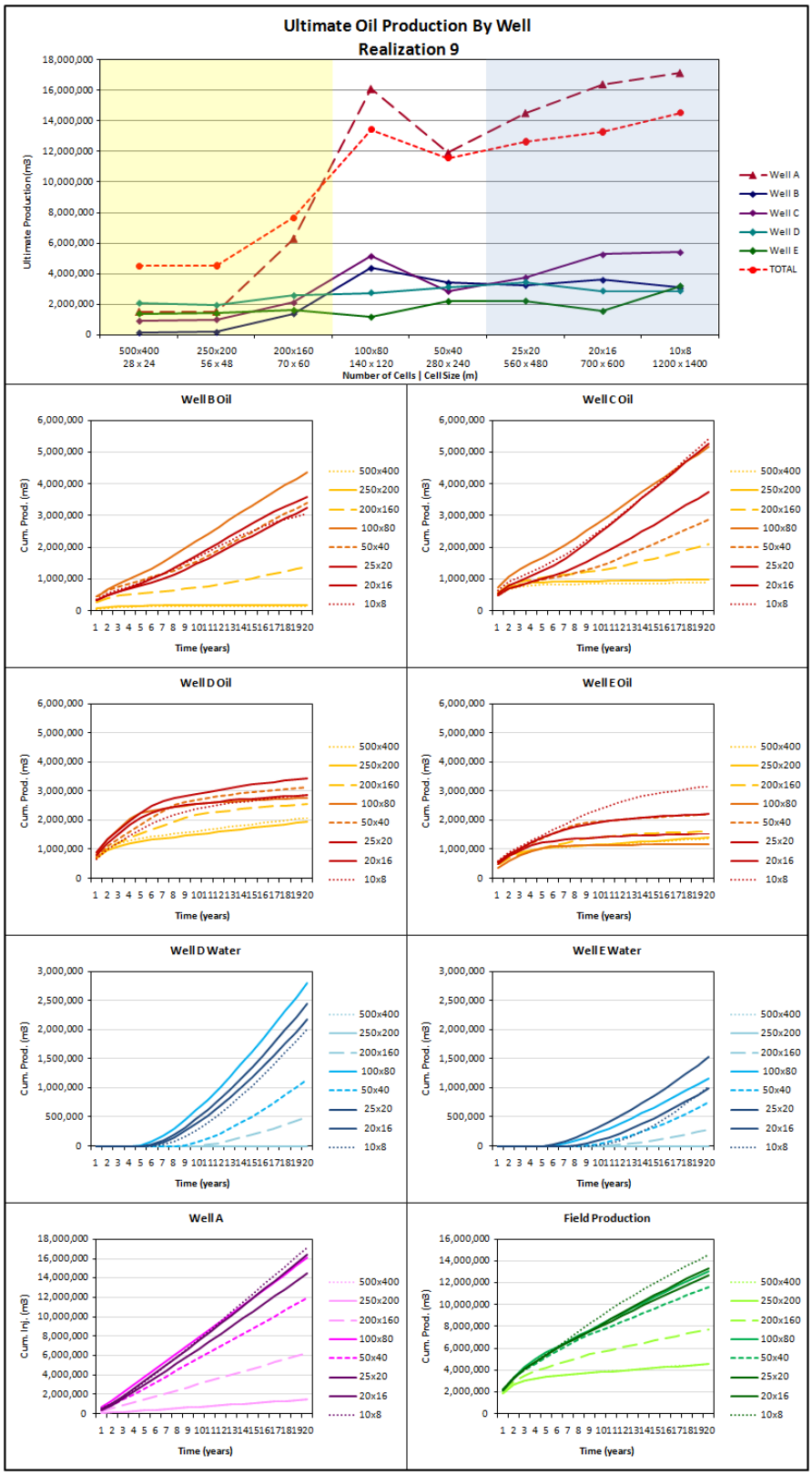

Figure 6.28. Realization 9, SQ100-25 scenario. The dramatic change in ultimate recovery between the 250 x 200 grid and the 200 x 80 grid is related to the change in properties around the injection well (Well A).